Geometric-phase-induced false electric dipole moment signals for particles in traps

J. M. Pendlebury,[1] W. Heil,[2] Yu. Sobolev,[2,*] P. G. Harris,[1] J. D. Richardson,[1] R. J. Baskin,[1] D. D. Doyle,[1] P. Geltenbort,[4] K. Green,[1,3] M. G. D. van der Grinten,[1,3] P. S. Iaydjiev,[3,†] S. N. Ivanov,[3,*] D. J. R. May,[1] and K. F. Smith[1]

[1]*Department of Physics and Astronomy, University of Sussex, Brighton, BN1 9QH, United Kingdom*

[2]*Institut of Physics, 55099 Mainz, Germany*

[3]*Rutherford Appleton Laboratory, Chilton, Didcot, OX11 0QX, United Kingdom*

[4]*Institut Laue Langevin, Boite Postale. 156, 38042 Grenoble, France*

(Received 14 February 2004; published 9 September 2004)

Theories are developed to evaluate Larmor frequency shifts, derived from geometric phases, in experiments to measure electric dipole moments (EDM's) of trapped, atoms, molecules, and neutrons. A part of these shifts is proportional to the applied electric field and can be interpreted falsely as an electric dipole moment. A comparison is made between our theoretical predictions for these shifts and some results from our recent experiments, which shows agreement to within the experimental errors of 15%. The comparison also demonstrates that some trapped particle EDM experiments have reached a sensitivity where stringent precautions are needed to minimize and control such false EDM's. Computer simulations of these processes are also described. They give good agreement with the analytical results and they extend the study by investigating the influence of varying surface reflection laws in the hard-walled traps considered. They also explore the possibility to suppress such false EDM's by introducing collisions with buffer gas particles. Some analytic results for frequency shifts proportional to the square of the **E** field are also given and there are results for the averaging of the **B** field in the absence of an **E** field.

DOI: 10.1103/PhysRevA.70.032102 PACS number(s): 11.30.Er, 13.40.Em, 14.20.Dh, 14.60.Cd

I. INTRODUCTION

The measurement of particle intrinsic electric dipole moments (EDM's) has been a significant physics activity for several decades [1,2]. Such dipole moments can exist only if parity (P) and time (T) reversal invariance are violated. The weak interaction violates P, while CP violation (equivalent to T violation from CPT invariance) is observed in the K and B meson systems [3–5]. The strength of these symmetry-violating interactions is very low compared with the strength of the "strong interaction" and the "electromagnetic interaction"; hence, the expected EDM's are very small. In the standard model of particle physics they are predicted to be much too small to be detected using current techniques. However, most suggested extensions to the standard model predict dipole moments that current advances in sensitivity of the experiments do make detectable [1,6]. It is also notable that CP violation outside of the standard model seems to be needed to explain the observed particle-antiparticle asymmetry of the Universe [7].

To improve levels of EDM measurement sensitivity requires ongoing vigilance with respect to false effects. That false electric dipole moment signals can arise from geometric phases (GP's), in particular, has been pointed out in the context of EDM measurements using atomic beams [8,9] where they have already been estimated to be a non-negligible source of error. We report here a theoretical analysis of GP-induced false EDM signals that can arise for *particles in traps* under a variety of conditions. Although the calculations are more complex than for beams, certain regularities in traps—for example, the isotropy of velocities and the uniform filling of the available phase space in mechanical equilibrium—allow us to obtain several explicit analytic results. We have also made extensive use of numerical modeling to verify all our analytic results to within a few normalized percent and to deal with some cases that are too complex to obtain anything other than approximate results by analytic methods. Agreement between analytic and numerical results does not necessarily validate the initial assumptions. However, in Sec. VI we present results for such false EDM signals from our experiments with trapped ultracold neutrons (UCN's) and cohabiting ^{199}Hg atoms, which agree with these calculations in sign and in magnitude to within an experimental error of 15%. We think this does validate the initial assumptions.

Most experiments to measure electric dipole moments observe the particles of interest as they move through a region permeated by uniform and aligned **E** and $\mathbf{B}_0$ fields. The particles being studied are generally neutral and have a total spin angular momentum **J**. The external field interaction Hamiltonian is

$$H_{ext} = -\frac{\mu_a}{J}\mathbf{J}\cdot\mathbf{B}_0 - \frac{d_a}{J}\mathbf{J}\cdot\mathbf{E}, \tag{1}$$

where μ_a and d_a are the magnetic and electric dipole moments, respectively. For static particles and fields, the transition frequencies between adjacent spin states J, M_J and J, $M_{J\pm1}$, which are also the Larmor precession frequencies, are for parallel and antiparallel $\mathbf{B}_0$ and **E**, given by the expressions

*On leave of absence from PNPI, St. Petersburg, Russia.

†On leave of absence from INRNE, Sofia, Bulgaria.

$$\omega_{L\uparrow\uparrow} = -\frac{(\mu_a B_{0\uparrow\uparrow} + d_a E)}{J\hbar}, \quad \omega_{L\uparrow\downarrow} = -\frac{(\mu_a B_{0\uparrow\downarrow} - d_a E)}{J\hbar}. \quad (2)$$

The experiments measure the accumulated phases $|\omega_{L\uparrow\uparrow}|T$ or $|\omega_{L\uparrow\downarrow}|T$ for the Larmor spin precession in the time of observation T, usually by using the Ramsey-separated oscillatory field magnetic resonance method [10]. According to Eqs. (2) an EDM d_a will reveal itself by causing a diminution or an augmentation of this accumulated precession phase according to whether the fields are as $\uparrow\uparrow$ or as $\downarrow\downarrow$. We will use the convention throughout that all angular displacements in the xy plane and all precession ω values will be positive if their associated axial vectors are in the same direction as $\mathbf{B}_0$.

If the particles are moving and the fields are static, but not completely uniform, there is some motion of the fields in the frame of any particle. The precession of the total spin of the ensemble can then include GP's (cf. Berry's phase [11]). Such phases are generally independent of the precession caused by an EDM, so they must be allowed for to avoid them being interpreted as an EDM falsely. Thus we should add the terms $+\varepsilon_{geo\uparrow\uparrow}/T$ and $+\varepsilon_{geo\uparrow\downarrow}/T$, respectively, to the right-hand sides (RHS's) of Eqs. (2). For the accumulated phases measured in the interval T, we now have the relation

$$(|\omega_{L\uparrow\uparrow}| - |\omega_{L\uparrow\downarrow}|)T = \frac{|\mu_a|(B_{0\uparrow\uparrow} - B_{0\uparrow\downarrow})T}{J\hbar} \pm \frac{2d_a ET}{J\hbar} \pm (\varepsilon_{geo\uparrow\uparrow} - \varepsilon_{geo\uparrow\downarrow}). \quad (3)$$

In each term in Eq. (3) the sign alternative has to be chosen to be the same as the sign of μ_a. Assuming for now that B_0 does not change in magnitude when **E** is reversed, the first term on the RHS of Eq. (3) will be zero. If the second (EDM) term is too small to measure and a GP term is present and is proportional to E and it is mistaken for the EDM term, one would find a false EDM d_{af} given by the equations

$$d_{af} = -(\varepsilon_{geo\uparrow\uparrow} - \varepsilon_{geo\uparrow\downarrow})\frac{J\hbar}{2ET} = -(\Delta\omega_{geo\uparrow\uparrow} - \Delta\omega_{geo\uparrow\downarrow})\frac{J\hbar}{2E}, \quad (4)$$

where $\Delta\omega_{geo\uparrow\uparrow}$ is the average rate of accumulation of the GP proportional to E for the particle ensemble spin in parallel fields.

The interaction of the particle spin with the **E** field that is of relevance in creating a GP is that of μ_a with the effective **B** field,

$$\mathbf{B}_v = \frac{\mathbf{E} \times \mathbf{v}}{c^2}, \quad (5)$$

arising from the particle velocity v. This is independent of the interaction of a genuine EDM with the **E** field. The effective field strength B_v is generally several orders of magnitude less than the main field strength B_0 and so it is "small" and it is in the xy plane and is generally comparable to the spatially varying xy components of the field $\mathbf{B}_0$ that are inevitably present as a feature of its small inhomogeneities. We shall find that a gradient $\partial B_{0z}/\partial z$ illustrated in Fig. 1 is particularly relevant. In the case of cylindrical symmetry it has the associated components in the xy plane,

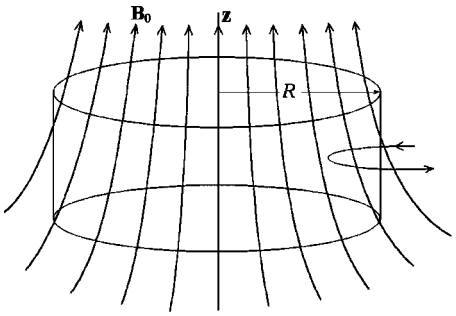

FIG. 1. (Color online) The shape of the $\mathbf{B}_0$ field lines, when there is a positive gradient $\partial B_{0z}/\partial z$, shown in relation to an outline of the trap used to store ^{199}Hg atoms and UCN's for the neutron EDM measurements at the ILL. If another field is superimposed having lines that both enter and leave through the sidewalls, like the one on the right-hand side, it will be shown later that it does not affect the false EDM signals that are generated.

$$\mathbf{B}_{0xy} = \mathbf{B}_{0r} = -\left(\frac{\partial B_{0z}}{\partial z}\right)\frac{\mathbf{r}}{2}, \quad (6)$$

at all radial positions **r** relative to the axis of symmetry. A GP is caused by the collaborative action of these two types of $\mathbf{B}_{xy}$ components: those from $\mathbf{B}_0$, which we will at times refer to as **a**, and those from $\mathbf{B}_v$, which we will at times refer to as **b**. Thus, we have

$$\mathbf{B}_{xy} = (\mathbf{B}_{0xy} + \mathbf{B}_v) = (\mathbf{a} + \mathbf{b}). \quad (7)$$

All these fields are varying with position in the trap. Inhomogeneities of **E**, unless gross, give small modulations of the already small $\mathbf{B}_v$ field and thus the modulations can be taken to be second order small. We will not consider the inhomogeneities of **E** any further in this paper, but the case of gross inhomogeneities of **E** is probably worth future investigation.

The particles are assumed to be moving in conditions where $mc^2 \gg mv^2 \gg |\mu_a B_0|$. Thus, no relativity is needed other than Eq. (5) Also, given the second condition and the fact that only the expectation values of the trapped particle spin direction are required, we can rely entirely on classical methods to calculate the spin motion using the equation

$$d\mathbf{J} = \frac{\mu_a}{J\hbar}[\mathbf{J} \times (\mathbf{B}_v + \mathbf{B}_0)]dt. \quad (8)$$

Our later results will only be dependent on the quantum number J through the simple factor of J in Eqs. (2) and (3). We shall use the normal convention that $(\mu_a/J\hbar)$ is called γ.

II. RAMSEY-BLOCH-SIEGERT SHIFTS FOR TRAPPED PARTICLES IN E PLUS B FIELDS

For particles exhibiting equilibrium motion in a trap, we will show that the combined action of the fields mentioned above is such that the particles experience a continuous rotation of the total component $\mathbf{B}_{xy}$ of Eq. (7) with a definite sense of rotation linked to the sense of **E**. Such rotating fields modify the rate of Larmor precession as can be deduced from the results of Ramsey [12] which generalized the results of

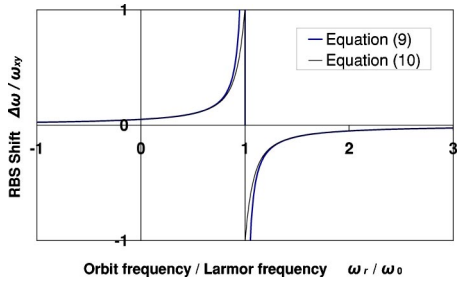

FIG. 2. (Color online) The Ramsey-Bloch-Siegert Larmor frequency shift $\Delta\omega$ caused by adding a field $\mathbf{B}_{xy}$ rotating in the xy plane, plotted against the angular frequency of rotation. The Larmor frequency, before the addition of $\mathbf{B}_{xy}$, was ω_0. The shift given by Eq. (9) goes to infinity, but that from Eq. (10) has a peak value of ω_{xy}.

Bloch and Siegert [13]. This change of precession rate is related to the buildup of a GP. The sign of this GP is linked to the sense of rotation of $\mathbf{B}_{xy}$ and, therefore, also to the sense of $\mathbf{E}$. At a given particle speed, we find that the rate of sweep of area B_xB_y by the $\mathbf{B}_{xy}$ field and the associated rate of buildup of GP are *not* very strongly dependent on the particular trajectory of a particle in a flat-bottomed hard-walled trap. Indeed, in the regime of Sec. IV A, confirmed by the results of Sec. IV D, we find that the rate of accumulation of GP in the adiabatic case is almost completely independent of which trajectory a trapped particle is following.

Ramsey considered a neutral particle with spin and magnetic moment precessing steadily with an angular velocity $\omega_L=\omega_0=-\gamma B_{0z}$ in a constant magnetic field $\mathbf{B}_{0z}$ and then the addition of a magnetic field of strength B_{xy} in the xy plane rotating in the plane at angular speed ω_r. He found that ω_L is shifted away from ω_0. To first order, this shift $\Delta\omega=\omega_L-\omega_0$ is given by

$$\Delta\omega=\frac{\omega_{xy}^2}{2(\omega_0-\omega_r)}, \tag{9}$$

where $\omega_{xy}=-\gamma B_{xy}$ [12]. We shall refer to this as the Ramsey-Bloch-Siegert (RBS) shift. The signs of the ω's must be followed carefully and by our convention are positive when the vector representing the sense of the circular motion of precession points to positive z. The shift $\Delta\omega$ is plotted in Fig. 2. The shift of Eq. (9) goes to infinity at $\omega_r=\omega_0$. However, the exact expression for the shift in the Larmor frequency [12] also shown in Fig. 2 is

$$\Delta\omega=\sqrt{(\omega_0-\omega_r)^2+\omega_{xy}^2}-(\omega_0-\omega_r), \tag{10}$$

where the negative root is taken, when necessary, to maintain agreement with the sign of Eq. (9). This result for $\Delta\omega$ peaks at the value $\Delta\omega=\omega_{xy}$. We will be interested in cases where $B_{xy}\approx 10^{-3}B_{0z}$ and $\omega_{xy}\approx 10^{-3}\omega_0$. A series expansion of the accurate expression for the shift shows that Eq. (9) uses the first term and that the second term is equal to the first term multiplied by $\omega_{xy}^2/[4(\omega_0-\omega_r)^2]\approx 10^{-6}$, except when ω_r is very close to (within $10^{-3}\omega_0$ of) ω_0. Thus, Eq. (9) is very accurate for most of our purposes. The range of the discrepancy in Fig. 2 is increased to 10% of ω_0 since it is drawn for the case $\omega_{xy}/\omega_0=10^{-1}$.

There are two distinct regimes $|\omega_r|<|\omega_0|$ and $|\omega_r|>|\omega_0|$, both of which are relevant. In the next section, we find that $|\omega_r|\approx(|v_{xy}|/R)$ where R is the radius of the trap in the xy plane and v_{xy} is the particle velocity component in the xy plane. The stored UCN's, as used in the neutron EDM measurements [15,16], fall into the regime $|\omega_r|<|\omega_0|$, while the atoms of the ^{199}Hg [17] and ^{3}He [18,19] comagnetometers fall into the regime $|\omega_r|>|\omega_0|$. It is only the case $|\omega_r|\ll|\omega_0|$ that can be considered to be *adiabatic* with E-field-dependent shifts that can be related to Berry's phase [11]. The shifts in the cases $|\omega_r|\approx|\omega_0|$ and $|\omega_r|>|\omega_0|$ are nonadiabatic GP's. The case $\omega_r=0$ gives a finite shift $\Delta\omega(0)$ which by Eq. (9) corresponds to the first-order term in the expansion in ω_{xy} for the addition of a *static* field $\mathbf{B}_{xy}$ at right angles to $\mathbf{B}_{0z}$, while Eq. (10) is exactly that addition. As ω_r increases from zero in the same sense as ω_0, $\Delta\omega$ increases and $[\Delta\omega(\omega_r)-\Delta\omega(0)]$ equals the rate of accumulation of Berry's phase as the total $\mathbf{B}$ vector revolves round a cone at the rate ω_r.

It is also useful to note that the numerator ω_{xy}^2 in Eq. (9) is

$$\omega_{xy}^2=\gamma^2\mathbf{B}_{xy}^2=\gamma^2(\mathbf{a}^2+\mathbf{b}^2+2\mathbf{a}\cdot\mathbf{b}). \tag{11}$$

Thus, there are three parts to the RBS shift; the first term $\mathbf{a}^2$ concerns the influence of $\mathbf{B}_{0xy}$ on ω_L in the absence of an $\mathbf{E}$ field. In the limit $|\omega_r|\gg|\omega_0|$, one finds, for example, that the contribution to ω_L from $\mathbf{B}_{0xy}$ becomes greatly attenuated so that, in the absence of an $\mathbf{E}$ field, ω_L remains close to $\omega_0=-\gamma B_{0z}$, to be compared with $\omega_L=-\gamma B_0$ when the particles are moving slowly. The second term $\mathbf{b}^2$, proportional to $(\mathbf{E}\times\mathbf{v})^2$, is involved in the calculation of the shift, proportional to E^2, that is called the second-order $(\mathbf{E}\times\mathbf{v})$ shift [14]. The term $2\mathbf{a}\cdot\mathbf{b}$, is the one that causes the GP shifts linear in E. In Sec. III we will describe a preliminary model that leads to some specific formulas for the effects of GP's in an ensemble of particles moving with an isotropic distribution of velocities. In particular, we will study the case of a gradient $\partial B_{0z}/\partial z$ that is constant over the trap volume. This is perhaps the most important case for this phenomenon, but it is not the only case, and in Sec. IV B we derive a more general assessment of the capacity for the $\mathbf{B}_0$ field to generate false EDM's. Even there, however, the conclusion is that it is the *volume-averaged* $\partial B_{0z}/\partial z$ which is all important. After outlining the preliminary model below, we shall refine it and give more comprehensive results in Sec. IV. In Sec. V we shall present the results of numerical simulations including those for the effects of inter particle collisions with buffer gases.

III. PRELIMINARY MODEL TO PREDICT GP SHIFTS IN TRAPS

Consider a particle (neutron or atom of ^{199}Hg) in a cylindrical storage vessel with the shape shown in Fig. 1 that follows the general layout of the neutron EDM (nEDM) apparatus at the ILL [15]. The z axis along which the volume average of $\mathbf{B}_0$ lies, pointing to positive z, is to a very good approximation along the cylinder axis of the trap. The circu-

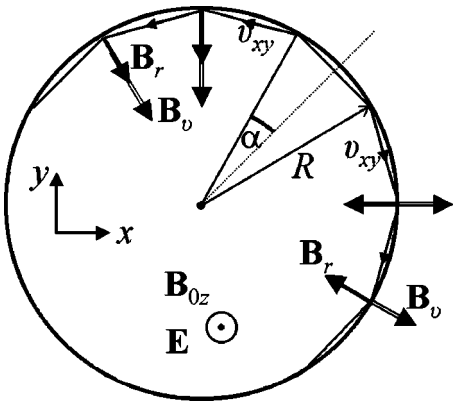

FIG. 3. (Color online) A view of the *xy* plane of the trap bounded by the circular sidewall. Part of an orbit is shown projected onto the *xy* plane for a particle undergoing specular reflection. The orbit is characterized by the angle α. Vectors $\mathbf{E}$ and $\mathbf{B}_{0z}$ point towards the reader and $\partial B_{0z}/\partial z$ is positive.

lar electrodes forming the roof and floor of the trap are *xy* planes and the cylindrical sidewalls are insulating. In this first approach, we assume fully specular reflection of the particles at all the trap surfaces and no particle-particle collisions. The *z* component of the particle velocity, being parallel to $\mathbf{E}$, does not contribute to $(\mathbf{E}\times\mathbf{v})$—i.e., to $\mathbf{b}$—and so does not contribute to the GP's under investigation. In fact, we may assume that the particle is confined to the *xy* plane moving with velocity v_{xy}. The $\mathbf{B}_0$ field is taken to be nearly uniform with a very small gradient $\partial\mathbf{B}_{0z}/\partial z$ that is to first order independent of position. It follows from Maxwell's equation div $\mathbf{B}=0$ that there exist inevitably the field components $\mathbf{B}_{0xy}=\mathbf{B}_{0r}=-(\partial B_{0z}/\partial z)(\mathbf{r}/2)=B_{0r}(\mathbf{r}/r)$, as in Eq. (6). In Fig. 3 we show a particular particle trajectory close to the cylinder wall. In the limit of getting very close to the wall with a very small angle α, $\mathbf{B}_{0r}$ and $\mathbf{B}_v$ are virtually parallel and aligned with the radius $\mathbf{r}$. Thus, a particle moving along such a trajectory sees rotating radial magnetic fields of amplitudes;

$$\text{for } \mathbf{B}_0 \ \&\ \mathbf{E}\uparrow\uparrow,\ B_{xy+}=B_{0r}-|B_v|,\ B_{xy-}=B_{0r}+|B_v|, \tag{12}$$

$$\text{for } \mathbf{B}_0 \ \&\ \mathbf{E}\uparrow\downarrow,\ B_{xy+}=B_{0r}+|B_v|,\ B_{xy-}=B_{0r}-|B_v|, \tag{13}$$

where the case $(+)$ is the sense of circulation with the orbit angular momentum vector parallel to $\mathbf{B}_0$ and the case $(-)$ is the opposite sense. This peripheral, or "garland," orbit has $|\omega_r|=v_{xy}/R$ where R is the radius of the trap. Collecting these small relations, we have

$$|B_v|=\frac{|v_{xy}||E|}{c^2},\ |\omega_0|=|\gamma B_{0z}|,\ |\omega_r|=\frac{|v_{xy}|}{R},$$

$$B_{0r}\to\{B_{0R}=-(\partial B_{0z}/\partial z)(R/2)\}\ \text{as}\ \alpha\to 0. \tag{14}$$

These rotating fields induce shifts in the Larmor frequency as given in Eq. (9). When mechanical equilibrium has been reached in the trap, any orbit will have equal probability of occupation for the two senses of circulation. Since we are ultimately interested in the ensemble average shift, we characterize the orbit by an equally weighted average of the shifts for the two senses of circulation. The result is that

$$\Delta\omega=\frac{(\gamma B_{xy+})^2}{4(\omega_0-|\omega_r|)}+\frac{(\gamma B_{xy-})^2}{4(\omega_0+|\omega_r|)}, \tag{15}$$

where the necessary sign links have been made. The result for $\Delta\omega$ has a sign that must be taken into account subsequently. Inserting Eqs. (12) and (13) into Eq. (15) we find that

$$\Delta\omega_{\uparrow\uparrow}=\frac{\gamma^2(B_{0R}^2+B_v^2)}{4}\left[\frac{1}{(\omega_0-|\omega_r|)}+\frac{1}{(\omega_0+|\omega_r|)}\right]-\frac{\gamma^2 B_{0R}|B_v|}{2}\left[\frac{1}{(\omega_0-|\omega_r|)}-\frac{1}{(\omega_0+|\omega_r|)}\right], \tag{16}$$

$$\Delta\omega_{\uparrow\downarrow}=\frac{\gamma^2(B_{0R}^2+B_v^2)}{4}\left[\frac{1}{(\omega_0-|\omega_r|)}+\frac{1}{(\omega_0+|\omega_r|)}\right]+\frac{\gamma^2 B_{0R}|B_v|}{2}\left[\frac{1}{(\omega_0-|\omega_r|)}-\frac{1}{(\omega_0+|\omega_r|)}\right]. \tag{17}$$

The upper line is the same for both Eqs. (16) and (17); i.e., it is independent of the direction of $\mathbf{E}$ and it represents the strengthening of the $\mathbf{B}_{0z}$ by the addition of $\mathbf{B}_{xy}$. The term B_{0R}^2 brings the precession rate to the full value for B_0 when $|\omega_r|\ll|\omega_0|$; the term B_v^2 represents the second-order $(\mathbf{E}\times\mathbf{v})^2$ shift proportional to E^2. As noted earlier, it is only the cross terms involving $B_{0R}\,|B_v|$ that create the GP that is linear in E. We now see that

$$(\Delta\omega_{\uparrow\uparrow}-\Delta\omega_{\uparrow\downarrow})=-\gamma^2 B_{0R}|B_v|\left[\frac{1}{(\omega_0-|\omega_r|)}-\frac{1}{(\omega_0+|\omega_r|)}\right]=-2\gamma^2 B_{0R}|B_v|\frac{|\omega_r|}{(\omega_0^2-\omega_r^2)}. \tag{18}$$

The factor $(\omega_0^2-\omega_r^2)^{-1}$ has a sharp peak and changes sign at the boundary between the ranges $|\omega_r|<|\omega_0|$ and $|\omega_r|>|\omega_0|$.

A. False EDM's for the nearly adiabatic case $|\omega_r|<|\omega_0|$

Recent neutron EDM measurements with UCN's [15,16] have come into this regime having values of $(|\omega_r|/|\omega_0|)$ of 0.06 and 0.04, respectively. For this case it is convenient to arrange Eq. (18), without approximation, in the form

$$(\Delta\omega_{\uparrow\uparrow}-\Delta\omega_{\uparrow\downarrow})=-2\gamma^2 B_{0R}|B_v|\frac{|\omega_r|}{\omega_0^2}\left[1-\frac{\omega_r^2}{\omega_0^2}\right]^{-1}. \tag{19}$$

Identifying the left-hand side (LHS) of Eq. (19) with $(\Delta\omega_{geo\uparrow\uparrow}-\Delta\omega_{geo\uparrow\downarrow})$ of Eq. (4) and making use also of Eqs. (4) and (14) we find that

$$d_{af}=-\frac{J\hbar}{2}\left(\frac{\partial B_{0z}/\partial z}{B_{0z}^2}\right)\frac{v_{xy}^2}{c^2}\left[1-\frac{\omega_r^2}{\omega_0^2}\right]^{-1} \tag{20}$$

for particles moving in peripheral orbits. For the *n*EDM experiments mentioned above, the final factor in square brack-

ets only differs from unity by about 0.5%. The ensemble of trapped UCN's in mechanical equilibrium will have an isotropic distribution of velocities for which $\langle v_{xy}^2\rangle=\langle v_x^2\rangle+\langle v_y^2\rangle=(2/3)\langle v^2\rangle$, a result that may be used for substitution in Eq. (20). The sign on the RHS is independent of the sign of the magnetic moment of the particle and so it gives a d_{af} with a sign opposite to that of $\partial B_{0z}/\partial z$. It will be shown in Secs. V and VI that the trap experiments are reaching the sensitivity where precautions are needed to avoid significant systematic errors arising from this mechanism.

To link the result with the Berry phase, we note that the first line of Eq. (18) concerns the difference between two shifts that differ in magnitude by a small amount. This difference gives the final result after subtraction and it exists because the two shifts come from fields in the *xy* plane that are rotating with opposite senses. The part of the shift which cancels in the subtraction is that part of the shift which would occur on adding the same field without rotation. Thus the part outside the square brackets in Eq. (19) can be shown to be quantitatively equal to the rate of accumulation of Berry's phase averaged over the two senses of circulation.

The term in square brackets shows that there is a giant resonance as $|\omega_r|\rightarrow|\omega_0|$. In the Berry phase approach, this may be thought of as being associated with the breakdown of adiabaticity causing the result to depart from the Berry result, which obtains only when the square brackets are unity.

B. False EDM's for the nonadiabatic case $|\omega_r|>|\omega_0|$

This case can occur with trapped atoms and molecules with energies above 100 mK and having magnetic moments at the nuclear magneton scale—for example, ^{199}Hg [17] and ^{3}He [18,20]. Later, we shall show that the effects can be suppressed by having a suitably high buffer gas pressure or a sufficiently small trap radius. The convenient arrangement of Eq. (18) for the case $|\omega_r|>|\omega_0|$ is

$$(\Delta\omega_{\uparrow\uparrow}-\Delta\omega_{\uparrow\downarrow})=2\gamma^2B_{0R}|B_v|\frac{1}{|\omega_r|}\left[1-\frac{\omega_0^2}{\omega_r^2}\right]^{-1}. \qquad (21)$$

Identifying the LHS of Eq. (21) with $(\Delta\omega_{geo\uparrow\uparrow}-\Delta\omega_{geo\uparrow\downarrow})$ of Eq. (4) and making use also of Eqs. (4) and (14) we find that

$$d_{af}=\frac{J\hbar}{2}\left(\frac{\partial B_{0z}}{\partial z}\right)\frac{\gamma^2R^2}{c^2}\left[1-\frac{\omega_0^2}{\omega_r^2}\right]^{-1} \qquad (22)$$

for particles moving in peripheral orbits. The analysis in Sec. IV shows that the RHS of Eq. (22) must be multiplied by a further factor of $1/2$ to convert it to the ensemble average over all types of orbits representing a uniform particle density distribution and an isotropic distribution of velocities in the trap. We note that γ is in units of radian/s. Relative to that given by Eq. (20) for the other regime, the sign of the false EDM has now changed due to the factor $(\omega_0^2-\omega_r^2)^{-1}$.

The d_{af} for peripheral orbits and particle speeds covering both regimes are plotted in Fig. 4, which shows a very close agreement between the results of numerical simulations and those of Eqs. (20) and (22). For the ^{199}Hg magnetometer used for the *n*EDM measurements at ILL [15,17] the factor $(\omega_0/\omega_r)^2\approx3\times10^{-3}$. We have measured a false EDM due to GP's in this magnetometer and it agrees, as predicted, with half the value given by Eq. (22). The agreement is to within the experimental error of ±15% arising out of the measurements of d_{af} and the precision with which an independently measured $\partial B_{0z}/\partial z$ was set up for the purpose (see Sec. VI).

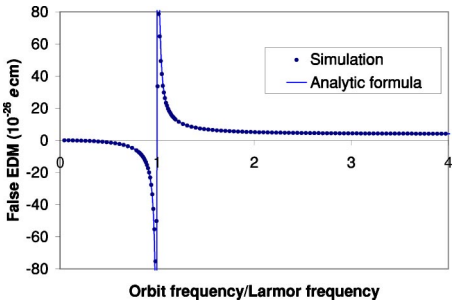

FIG. 4. (Color online) The false EDM for a particle in a peripheral orbit as its speed is increased. The value of $\partial B_{0z}/\partial z=+1$ nT/m; the holding field B_{0z} is 1×10^{-6} T. At the extreme left of the figure, the gyromagnetic ratio γ is unimportant and the same results are obtained for any particle. The values on the right are those for a γ^2 factor and a trap radius R (0.25 m) appropriate to the ^{199}Hg atoms in the ILL *n*EDM apparatus.

IV. ELABORATING THE MODEL

It has proved to be possible to solve the equations of motion of the expectation of the particle spin **J** for particles in an orbit with specular reflection in a circular trap, having any particular glancing angle of incidence α on the circular wall, and in a $\mathbf{B}_0$ field with a uniform $\partial B_{0z}/\partial z$ and cylindrical symmetry about the axis of the trap. The solution is valid for all values of $|\omega_r|/|\omega_0|$, except those very close to unity. The method and the results are presented in Sec. IV D below. Where there is an overlap the results obtained agree with the results obtained by simpler methods in the following Secs. IV A, IV B, and IV C.

A. Elaborations when $|\omega_r|<|\omega_0|$

We remark that the calculation in Sec. III might seem to be of limited validity in that (i) the $\mathbf{B}_{xy}$ field, while rotating slowly, does not maintain constant amplitude in any orbit other than that at the extreme periphery (in general, a series of triangles are swept in the B_xB_y plane), and (ii) for *all* of the orbits, the total $\mathbf{B}_{xy}$ field performs some of its rotation slowly and some of it, on reflection at the sidewall, instantaneously, as shown in Fig. 5.

Since we are concerned with the adiabatic regime, we can use the Berry phase approach. Concerning point (i) we make the following postulate: if the $\mathbf{B}_{xy}$ field rotates slowly through any small arc of area δA in the B_xB_y plane, a Berry phase is acquired as given by the usual formula appropriate to the solid angle $\delta\Omega=\delta A/B_{0z}^2$ (first-order expression). The original statement for the Berry phase refers only to complete circuits of the variables such as $\mathbf{B}_{xy}$. However, Samuel and Bhandari [21] showed that, in general, any change in the geometric parameters can introduce a geometric phase. We find that our postulate is borne out by computation and also

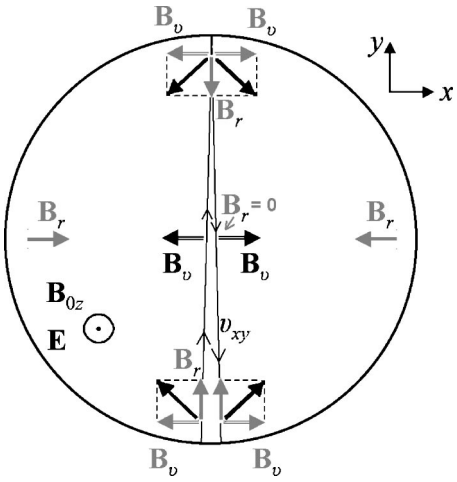

FIG. 5. (Color online) The $\mathbf{B}_{xy}$ fields (in black) seen by a particle going back and forth close to the y axis. Going towards positive y, the $\mathbf{B}_{xy}$ field rotates steadily anticlockwise by about 70° as drawn. The first reflection of the particle towards negative y causes an *instantaneous* anticlockwise rotation by about 110° as drawn. The same two rotations occur on the path to, and at, the second reflection. The size of the rotations depends on the size of B_{0r}/B_v.

analytically by considering a brief entry into the frame rotating at the same rate as $\mathbf{B}_{xy}$. In the computations, one has to separate the Berry phase from an oscillating projection phase arising from the fact that the spin is precessing around the total **B** field which is tilted relative to the laboratory z axis. The projection phase averages over time to zero except in so far as it can be said to play a role in the GP caused by the instantaneous jumps in angle of $\mathbf{B}_{xy}$ discussed below. Following the postulate, the rotation of $\mathbf{B}_{xy}$ combined with a change in the strength B_{xy} sweeping a triangular area A in the B_xB_y plane can be treated as an integral of successive small rotation arcs to justify that a total Berry phase is acquired corresponding to

$$\Omega = \frac{A}{B_{0z}^2}. \tag{23}$$

Coming now to point (ii), the rotation of $\mathbf{B}_{xy}$ is slow while the particle is in free flight along a chord path, but on reflection at the sidewall, $\mathbf{B}_{xy}$ rotates to a new direction in a time of the order 10^{-8} s, as a result of the change in direction of $\mathbf{B}_v$. The 10^{-8} s happens to apply to both neutron and ^{199}Hg atom reflections, and it is just an instant compared to the relevant Larmor periods, which are of the order of 10^{-2} s.

In Appendix A, Eq. (A6) it is shown that for a free path between trap surface positions 1 and 2 the field area swept *slowly*, after averaging over both forwards and backwards directions of travel along the path, is given, for the cylindrically symmetric trap and $\mathbf{B}_0$, by

$$A_{sl\uparrow\uparrow} = -B_{0R}|B_v|\sin\alpha. \tag{24}$$

Also, it is shown that the area $A_{i\uparrow\uparrow}$ that is swept *instantaneously* after averaging over both directions of travel for the path, Eq. (A8), is the same as the expression for $A_{sl\uparrow\uparrow}$ in Eq. (24). At first sight, one might think the instantaneous rotations of $\mathbf{B}_{xy}$ would do nothing because there is no time for **J** to move. However, we make our second postulate: that if an instantaneous jump in the direction of the **B** is followed by a sufficiently long interval of rest or slow motion of **B**, the expectation of **J**, after averaging over all starting phases, nevertheless acquires a GP of the usual value corresponding to the area swept. Most of this GP builds up over the first half Larmor period following the jump, but the GP overshoots and starts a decaying oscillation about the value it would have had for a slow rotation through the same angle. This statement relies on observations of our numerical computations (see Fig. 6). It can also be made plausible if one argues that the angular jump followed by a sufficiently long rest, amounting overall to an angular velocity less than ω_L, might reasonably lead to the usual adiabatic result.

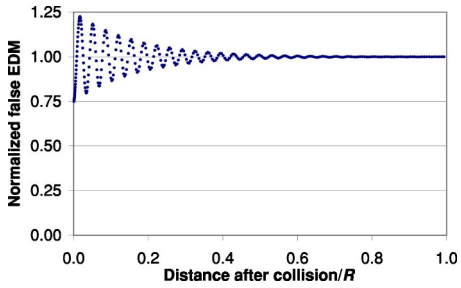

FIG. 6. (Color online) A transient oscillation following an instantaneous rotation of $\mathbf{B}_{xy}$ at a collision. The resulting false EDM settles down to the same value as it would have had if the head of the $\mathbf{B}_{xy}$ vector had followed a straight line slowly to the new position.

Adding the two equal areas swept as given in Eqs. (24), (A6), and (A8) and using Eq. (23) we obtain the GP

$$\Omega_{\uparrow\uparrow} = -\frac{2B_{0R}|B_v|\sin\alpha}{B_{0z}^2}. \tag{25}$$

The time to travel a path is $\Delta t = 2R\sin\alpha/v_{xy}$. Thus $\Delta\omega_{geo\uparrow\uparrow} = \Omega_{\uparrow\uparrow}/\Delta t = (B_{0R}|B_v|/B_{0z}^2)(v_{xy}/R)$ which is seen to be independent of α and, thus, the *same for all chord paths*. When **E** is reversed $|B_v|$ is replaced by $-|B_v|$ so that

$$(\Delta\omega_{\uparrow\uparrow} - \Delta\omega_{\uparrow\downarrow}) = -\frac{2B_{0R}|B_v|}{B_{0z}^2}\frac{|v_{xy}|}{R} = -2\gamma^2 B_{0R}|B_v|\frac{|\omega_r|}{\omega_0^2}. \tag{26}$$

Combining Eq. (26) with Eqs. (4) and (14) now recreates the leading term of Eq. (20), thus proving that Eq. (20) applies to all the orbits and so finally to an ensemble of particles encompassing all of the different orbits.

We return to pick up on one point from the foregoing; when the $\mathbf{B}_{xy}$ field rotates instantaneously the *actual* path of its motion is unimportant. All that matters are the initial and final positions. The resulting GP acquired is that which it would have acquired if the head of the $\mathbf{B}_{xy}$ vector had passed slowly by a *straight-line path* from the starting position to final position. This was the assumption made in calculating swept areas.

Concerning the breakdown of adiabaticity as ω_r approaches ω_0, it is tempting to assume that the square bracket

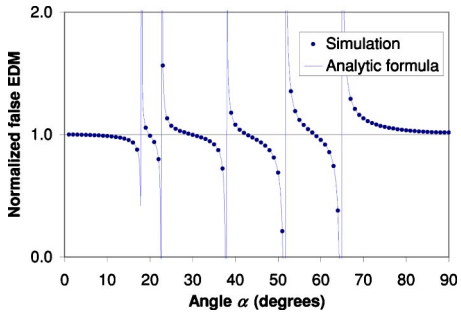

FIG. 7. (Color online) Computer simulation of resonances occurring as a function of trajectory angle α for UCN's with a constant speed $v_{xy}=5$ m/s and specular reflection, normalized to the value expected from Eq. (29) for a uniform spatial distribution of particles in the trap. The analytic formula is that given in Eq. (78). Away from the resonances d_{af} is independent of α.

resonance term of Eq. (20) can be adopted for the other orbits provided that one uses the appropriate ω_r, given by

$$\omega_r = \frac{2\alpha}{\Delta t} = \frac{v_{xy}\alpha}{R\sin\alpha}. \tag{27}$$

Thus, some dependence of the false EDM on α will appear when the breakdown of adiabaticity is significant. If the expansion $[1-(\omega_r/\omega_0)^2]^{-1}\approx 1+(\omega_r/\omega_0)^2$ suffices, we suggest that, for the case of an isotropic distribution of velocities and uniform filling of real space in the trap, ω_r^2 is replaced by a weighted average ω_r^{*2} which is obtained from the expression of Eq. (27) when averaged with the weight $(4/\pi)\sin^2\alpha$ for the probability of occupation of the orbits (see Appendix B). We find that

$$\omega_r^{*2} = \frac{\pi^2}{6}\left(\frac{v_{xy}}{R}\right)^2. \tag{28}$$

We now conclude that for an isotropic distribution of velocities and a uniform distribution in space the result

$$d_{af} = -\frac{J\hbar}{2}\left(\frac{\partial B_{0z}/\partial z}{B_{0z}^2}\right)\frac{v_{xy}^2}{c^2}\left[1-\frac{\omega_r^{*2}}{\omega_0^2}\right]^{-1} \tag{29}$$

will apply for cases where $\omega_r/\omega_0<0.2$ and there is partly diffuse reflection.

In the case of pure specular reflection, the analytic results of Sec. IV D, and the values, away from the resonances, given by our numerical simulations shown in Fig. 7, also confirm that in the adiabatic limit, Eq. (20) applies independently of the type of orbit considered and therefore to an ensemble uniformly filling the trap.

The existence of resonances in Fig. 7 is worth noting. The smooth rotation of the field is interrupted at regular intervals for the interjection of instantaneous rotations at each wall collision—i.e., at intervals Δt. The result is a sideband effect with the spectrum of rotational frequencies, $\omega_{sb}=\omega_r\pm k|\omega_s|$, $k=1,2,3,\ldots$, and $\omega_s=2\pi/\Delta t$. From Eq. (20) one anticipates that there will be resonances whenever $\omega_{sb}^2=\omega_0^2$, which in the regime $|\omega_r|<|\omega_0|$ occurs for the condition $\pm|\omega_r|=|\omega_0|-k|\omega_s|$. Generally, $|\omega_0|$ is fixed, but $|\omega_r|$ and $|\omega_s|$ depend on v_{xy}, which will usually span a continuous range between zero and v, and also on α, giving a wide range of tuning via the choice of orbit. This tuning is needed to obtain the exact resonance condition. Thus the sideband resonances can be seen in the case of specular reflection and rather specific orbits as illustrated in Fig. 7. The resonances have a dispersive shape for the d_{af} produced if one tunes through them by varying v_{xy} or α. These resonances are reproduced by the more comprehensive solution of Sec. IV D, Eq. (78) In the practical conditions of an ensemble of particles the resonances will tend to average away due to the presence simultaneously of a wide range of values of v_{xy}. Diffuse reflection at the walls also suppresses the resonances by causing frequent random changes in α and the chord travel times.

B. Case $|\omega_r|<|\omega_0|$ and all shapes of $\mathbf{B_0}$

Here, a method is developed for assessing the magnitude of the GP linear in E that will stem from *any* shape of small inhomogeneity in the $\mathbf{B}_0$ field. At the same time, we can generalize to all shapes of trap provided that the electrodes are plane parallel and the sidewalls are perpendicular to the electrodes. We have argued above that, in this regime, each free path produces its own GP that is independent of the previous path. Furthermore, we find using Eqs. (A5) and (A7) that the magnitude of this GP is given in terms of values at the two ends 1 and 2 of the path as

$$\varepsilon_{geo\uparrow\uparrow} = -(B_{0xyn1}\sin\alpha_1 + B_{0xyt2}\sin\alpha_2)\frac{|B_v|}{B_{0z}^2} - (B_{0xyt1}\cos\alpha_1 - B_{0xyt2}\cos\alpha_2)\frac{|B_v|}{2B_{0z}^2}, \tag{30}$$

where α_1 and α_2 are the angles (always taken to be positive) between the particle path with the sense $1\rightarrow 2$ projected onto the xy plane and the tangents to the surface at the ends which point in the direction of $\mathbf{z}\times\mathbf{n}$, where $\mathbf{z}$ is in the direction of the positive z axis and $\mathbf{n}$ is in the direction of the outward normal to the surface at the end concerned (see Fig. 16). In the case of a cylindrical trap α_1 and α_2 are equal to each other and to α as used in earlier sections, but for other shapes of trap they may not be equal. B_{0xyn} is the component of $\mathbf{B}_{0xy}$ in the direction of the outward normal to the surface and B_{0xyt} is the component of $\mathbf{B}_{0xy}$ in the direction tangential to the surface just specified. We note particularly that B_{0xyn} is always zero at the electrode surfaces since these are xy planes.

We now focus on a small area of surface of the trap dA_1 at end 1 and on all the free paths starting out from dA_1. The form of the above expression suggests that the GP's accumulated for a path after averaging over the two possible directions of travel can be regarded as having two contributions, each one associated with a specific end of the path. The contribution from end 1 is

$$\varepsilon_{geo\uparrow\uparrow 1} = -\left[\frac{B_{0xyn1}\sin\alpha_1|B_v|}{B_{0z}^2} - \frac{B_{0xyt1}\cos\alpha_1|B_v|}{2B_{0z}^2}\right] \tag{31}$$

per particle departing from the surface. We next calculate the rate of injection of GP's into the whole ensemble of N particles in the trap that is coming from the rate of departure of

all particles from the area element dA_1 and then later integrate this over all the wall area. Our particles all have speed v and their velocities have an isotropic distribution of directions. For the directions we use θ (0 to π) as the polar angle from the z axis and α_1 (0 to π) as the azimuthal angle about the z axis. We integrate using a velocity element defined by the ranges $d\theta$ and $d\alpha_1$ at angles θ and α_1 and note that $v_{xy} = v \sin\theta$ and $v_n = v_{xyn} = v \sin\theta \sin\alpha_1$.Thus the rate of acquisition of GP's by the ensemble expressed as the integral of particle flux times GP's is

$$N\omega_{geo\uparrow\uparrow} = -2\oint_{A_s}\int_0^{\pi}\int_0^{\pi}\frac{n\sin\theta\, d\theta\, d\alpha_1}{4\pi} v\sin\theta\sin\alpha_1 \times\left[\frac{B_{0xyn1}\sin\alpha_1}{B_{0z}^2}+\frac{B_{0xyt1}\cos\alpha_1}{2B_{0z}^2}\right]\frac{v\sin\theta E}{c^2}dA_1, \tag{32}$$

where n is the number of particles per unit volume, $N = (nV)$ is the total number in the trap of volume V, and A_s is the total area of the sidewalls. The initial factor of 2 on the RHS of Eq. (32) is there to include, at the same time, the GP's injected by particles *arriving* at the surface dA_1 as well as those leaving it. The term $-B_{0xyt1}\cos\alpha_1$ gives zero when integrated over α_1 from 0 to π, showing that nowhere on the surface can B_{0xyt1} contribute to the GP. To find the total $\omega_{geo\uparrow\uparrow}$ the integration must be over *all* of the sidewall surface of the trap. All contributions from the electrode surfaces are zero. Finally we double the result again to obtain $(\Delta\omega_{geo\uparrow\uparrow} - \Delta\omega_{geo\uparrow\downarrow})$ and after combining with Eq. (4) find

$$d_{af} = +\frac{J\hbar}{2}\left(\frac{\langle B_{0xyn}\rangle A_s}{B_{0z}^2 V}\right)\frac{v_{xy}^2}{c^2}\left[1-\frac{\omega_r^{*2}}{\omega_0^2}\right]^{-1}, \tag{33}$$

except that the factor in square brackets has been inserted in an *ad hoc* way to represent the effect of the failure of adiabaticity as the collision frequencies approach ω_0. The square brackets are only valid here when $(\omega^*_r/\omega_0)^2 \ll 1$. The quantity $\langle B_{0xyn}\rangle$ is the average magnetic flux density normal to the sidewalls, and the key quantity $\langle B_{0xyn}\rangle A_s = \Phi_s$ is the net flux leaving through the sidewalls. In the specific case, with cylindrical symmetry, the more general equation (33) easily allows one to recover Eq. (20). Equation (33) applies for *any* shape of small distortions in $\mathbf{B}_0$ and *all* trap shapes having parallel electrodes and perpendicular sidewalls. Magnetic flux lines are always conserved so that $\Phi_s = -(\Phi_u + \Phi_l)$ in terms of the net outgoing magnetic flux lines from the sidewalls, the upper electrode, and the lower electrode, respectively. Magnetometers as proposed using ^{3}He [19] or neutrons [20] arranged to measure the **B** field averaged over thin disk-shaped volumes adjacent to the electrodes would, to a good approximation, measure $(\Phi_u + \Phi_l)$ and hence $-\Phi_s$ to help evaluate the RHS of Eq. (33). We also note that $\langle B_{0xyn}\rangle A_s/V$ is equal to the volume-averaged two-dimensional divergence $\langle \partial B_{0x}/\partial x + \partial B_{0y}/\partial y\rangle_V$ and to the volume-averaged $\langle -\partial B_{0z}/\partial z\rangle_V$. Taking this last form we have

$$d_{af} = -\frac{J\hbar}{2}\left(\frac{\langle \partial B_{0z}/\partial z\rangle_V}{B_{0z}^2}\right)\frac{v_{xy}^2}{c^2}\left[1-\frac{\omega_r^{*2}}{\omega_0^2}\right]^{-1}, \tag{34}$$

which is similar to Eq. (29) except that $\partial B_{0z}/\partial z$ has been replaced by its volume average and Eq. (34) can be used for any shape of $\mathbf{B}_0$ inhomogeneities.

C. Elaborations for the case $|\omega_r| > |\omega_0|$

First, we must deal properly with all the different orbits since, unlike the adiabatic regime, there is a change in the rate of accumulation of GP with the type of orbit. For example, the highly peripheral orbit gives 3 times more rate of accumulation of GP's than that of the other extreme where a particle goes to and fro across the diameter. The reason for the different behavior in this regime is as follows. There are two influences for change. The more peripheral orbits have lower $|\omega_r|$ and a higher average strength for $\mathbf{B}_{0xy}$. In the adiabatic regime these two influences on the rate of accumulation of GP's happen to cancel as the orbit α is changed. In the $|\omega_r| > |\omega_0|$ regime the effect of lowering $|\omega_r|$ is reversed and produces larger phase shifts, while the $\mathbf{B}_{0xy}$ field strength dependence on orbit is the same in both regimes. In the $|\omega_r| > |\omega_0|$ regime the effects of frequency and of field strength now reinforce so that the peripheral orbits generate the larger GP's.

We can obtain some quantitative results as follows. The particle spin **J** is precessing relatively slowly in the xy plane and we add a $\mathbf{B}_{xy}$ field which is rotating relatively quickly. The effect of the rotating field on the spin head makes it execute small sideways hops—one per complete turn of $\mathbf{B}_{xy}$. These accumulating hops across the xy plane give the rate of accumulating (nonadiabatic) GP's. In the limit $|\omega_0|/|\omega_r| \to 0$ the angular displacement produced in the hop associated with a completed turn of $\mathbf{B}_{xy}$ can be obtained accurately and analytically as follows. We rely on the independence of very small angular displacements about orthogonal axes. For any type of orbit, suppose the spin **J** starts parallel to the x axis and $\mathbf{B}_{xy}$ as seen by the particle in orbit has the periodically varying components $B_x(t)$ and $B_y(t)$. The first thing of importance is that the spin should be lifted out of the xy plane and to calculate this we use

$$J_z(t_1) = \int_0^{t_1}\gamma B_y(t) J\, dt. \tag{35}$$

As soon as J_z is finite **J** begins to acquire a component J_y by precession about B_x as given by

$$J_y(\tau) = \int_0^{\tau}\gamma B_x(t_1) J_z(t_1) dt_1, \tag{36}$$

where τ is the period for the orbit. The absolute angles in these movements of **J** are of the order of $(\gamma B_{xy}/|\omega_r|)$ radian. This will always be less than B_{xy}/B_{0z}, which is typically less than 10^{-3} so the independence of angular movements about orthogonal axes also has the accuracy 10^{-3}. Equations (35) and (36) indicate that the resultant hops are proportional to γ^2. The sense of the GP's acquired is independent of the sign of μ_a and is always opposite to the sense of rotation of $\mathbf{B}_{xy}$.

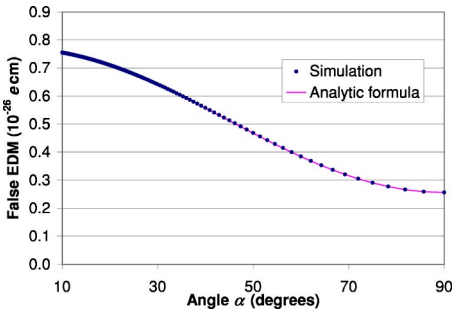

FIG. 8. (Color online) The dependence of the false EDM on the angle α characterising the orbit for the high velocity case $|\omega_r| \gg |\omega_0|$.

We have used Eqs. (35) and (36) to verify that in the limit $|\omega_0|/|\omega_r| \to 0$, a smoothly rotating $\mathbf{B}_{xy}$ field of constant amplitude reproduces the RBS shift of Eq. (9). The result is independent of the starting phase angle between $\mathbf{B}_{xy}$ and $\mathbf{J}$ in the xy plane. Next we applied the equations to the case of a particle passing to and fro along the diameter aligned with the x axis in parallel $\mathbf{E}$ and $\mathbf{B}_0$ fields for the case $\alpha = \pi/2$. On the outward path $t=0$ to $\tau/2$, $B_y(t) = +|B_v| = \text{const}$, and on the return path, $t=\tau/2$ to τ, $B_y(t) = -|B_v| = \text{const}$. Thus, $J_z(t_1)$ from Eq. (35) is a triangle function starting at 0 rising linearly as $\gamma|B_v|Jt_1$ to a peak of $\gamma|B_v|J\tau/2$, then falling linearly to zero again. In Eq. (36) on the outward pass $B_x(t_1) = -B_{0R}[1 - 4t_1/\tau]$ and for the return pass $\tau/2 \leqslant t_1 \leqslant \tau$, $B_x(t_1) = B_{0R}[3 - 4t_1/\tau]$. After completing the integrals of Eqs. (35) and (36) we find the GP acquired is $\varepsilon_{geo\uparrow\uparrow} = J_y(\tau)/J = B_{0R}|B_v|\tau^2/12$. Dividing out one factor of τ converts the result to $\Delta\omega_{\uparrow\uparrow}$. Hence $(\Delta\omega_{\uparrow\uparrow} - \Delta\omega_{\uparrow\downarrow}) = B_{0R}|B_v|\tau/6 = 2B_{0R}|B_v|R/(3v_{xy})$. Substituting with Eqs. (4) and (14) we find a d_{af} that is 1/3 of the leading term obtained in Eq. (22) for the highly peripheral orbit. A repeat of the calculations with $\mathbf{J}$ initially along the y axis with suitably modified equations leads to the same answer. Thus, we conclude that the initial phase of $\mathbf{J}$ does not affect the result.

We have used this method to obtain (tediously) results for three other closed orbits with $\alpha = 3\pi/8$, $\pi/4$, and $\pi/8$, respectively. The results are all consistent with the necessary multiplier for the RHS of Eq. (22) taking the form $(1 + 2\cos^2\alpha)/3$ for an orbit characterized by an angle α. The solution in Sec. IV D confirms that this formula applies to all orbits, whether or not they are closed, as do, also, the two-dimensional (2D) computer simulations shown in Fig. 8.

If the particle distribution in the trap is uniform in space and the velocities are isotropic, then the probability distribution function for the occupation of orbits characterized by α is $P(\alpha) = (4/\pi)\sin^2\alpha$ (see Appendix B). Averaging the multiplier $(1+2\cos^2\alpha)/3$ using the weight function $P(\alpha)$ yields 1/2. Thus, we need to *multiply* the RHS of Eq. (22) for the highly peripheral orbit by an additional factor of 1/2 to convert it to the form that represents this ensemble. Hence, for the ensemble we have

$$d_{af} = \frac{J\hbar}{4}\left(\frac{\partial B_{0z}}{\partial z}\right)\frac{\gamma^2 R^2}{c^2}\left[1 - \frac{\omega_0^2}{\omega_r^{\dagger 2}}\right]^{-1}, \tag{37}$$

where the square brackets are valid for $(\omega_0/\omega_r^{\dagger})^2 \ll 1$ and from the appropriate weighted average we find

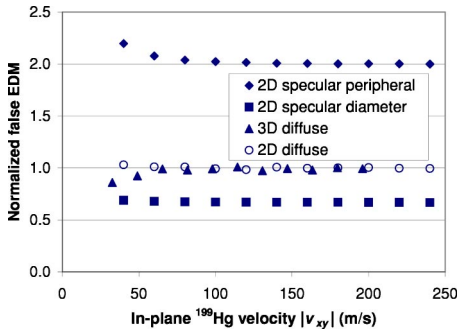

FIG. 9. (Color online) Results from computer simulations of the false EDM effect for ^{199}Hg atoms, in the cases of peripheral orbit, diameter orbit, and diffuse reflection in 2D and 3D, as a function of velocity. All results are normalized to the analytic result expected for diffuse reflection in the high-velocity limit.

$$\omega_r^{\dagger 2} = 0.65\left(\frac{v_{xy}}{R}\right)^2. \tag{38}$$

A comparison between Eq. (37) and computer simulations is shown in Fig. 9. The surprising new element in Fig. 9 is that the results for diffuse reflection show no detectable difference from those of Eq. (37), which was derived for specular reflection. We have also used computer simulations for $|\omega_r| \gg |\omega_0|$ to look for d_{af} signals from magnetic flux which both enters and leaves by the trap sidewalls—i.e., a $\mathbf{B}$ field with no 2D divergence in the xy plane and with $\langle \partial B_{0z}/\partial z\rangle_V = 0$. We found such flux to be at least a thousand times less effective in generating a d_{af} than the divergent flux associated with a finite $\partial B_{0z}/\partial z$. As yet, we have no theory, such as that in Sec. IV B, to confirm that d_{af} is always proportional to $\langle \partial B_{0z}/\partial z\rangle_V$ in the regime $|\omega_r| > |\omega_0|$.

D. Full solution for cylindrical symmetry, specular reflection, and all values of $|\omega_r|/|\omega_0|$

The classical motion of $\mathbf{J}$ can be solved more comprehensively for a cylindrical trap having specular reflection of the particles at all the walls and immersed in a *nearly* uniform $\mathbf{B}_0$ having cylindrical symmetry and a *small* uniform $\partial B_{0z}/\partial z$. For this case $\mathbf{B}_{0xy} = \mathbf{B}_r = -(\partial B_{0z}/\partial z)\mathbf{r}/2$. Our setups have $\Delta B_{0z}/B_{0z} < 10^{-3}$ over the height of the trap. The axes are chosen such that $\mathbf{x}\times\mathbf{y}$ is in the direction of $\mathbf{z}$ and the volume averaged $\mathbf{B}_0$ points the direction of $\mathbf{z}$. We will use $\varphi(t)$ for the angle of rotation of the spin component $\mathbf{J}_{xy}(t)$ towards the positive y axis starting on the positive x axis, with $\varphi(t) = 0$ at $t=0$. The equation of motion for the expectation value of $\mathbf{J}$ for a particle is $d\mathbf{J}/dt = \gamma[\mathbf{J}\times\mathbf{B}] = \gamma[\mathbf{J}\times(\mathbf{B}_v + \mathbf{B}_0)]$ and in components

$$dJ_x/dt = \gamma[J_y B_z - J_z B_y], \tag{39}$$

$$dJ_y/dt = \gamma[J_z B_x - J_x B_z], \tag{40}$$

$$dJ_z/dt = \gamma[J_x B_y - J_y B_x]. \tag{41}$$

Equations (39) and (40) contain the information about the rate of change of phase $\varphi(t)$ of $\mathbf{J}_{xy}$ in the xy plane since they

define the vector $d\mathbf{J}_{xy}$ for the interval dt. The component of $d\mathbf{J}_{xy}$ that is perpendicular to $\mathbf{J}_{xy}$ must be equal to $J_{xy}\,d\varphi$.

For the vectors concerned, we may write in components, ${J_{xy}}^2\,d\varphi=(\mathbf{J}\times d\mathbf{J})_z=(J_x\,dJ_y-J_y\,dJ_x)$. On substituting Eqs. (39) and (40) into this last expression, we obtain

$$\frac{d\varphi}{dt}=-\gamma B_z+\gamma\frac{J_z}{J_{xy}^2}[J_xB_x+J_yB_y]. \tag{42}$$

Since $\mathbf{B}_v$ does not contribute to B_z, we have $-\gamma B_z=-\gamma B_{0z}=\omega_0$. Introducing $\omega_x=-\gamma B_x$ and $\omega_y=-\gamma B_y$ and noting that $J_x=J_{xy}\cos\varphi$, $J_y=J_{xy}\sin\varphi$, Eq. (42) can become

$$\frac{d\varphi}{dt}-\omega_0=-\frac{J_z}{J_{xy}}[\omega_x\cos\varphi+\omega_y\sin\varphi]. \tag{43}$$

We now introduce $\phi=\varphi-\omega_0 t$, as the total phase minus the dynamic phase from B_{0z}—i.e., that part of the phase produced by the $\mathbf{B}_{xy}$ fields. Then Eqs. (41) and (43) become

$$\frac{dJ_z}{dt}=J_{xy}[\omega_x\sin(\phi+\omega_0t)-\omega_y\cos(\phi+\omega_0t)] \tag{44}$$

and

$$\frac{d\phi}{dt}=-\frac{J_z}{J_{xy}}[\omega_x\cos(\phi+\omega_0t)+\omega_y\sin(\phi+\omega_0t)]. \tag{45}$$

We make the following points: (i) that ϕ grows approximately linearly from zero and even in the extreme cases does not exceed 0.03 rad by the end of the Ramsey interval T. Over times comparable with the Larmor period, ϕ only varies by about 10^{-5} rad. The role of ϕ on the RHS of Eqs. (44) and (45) is to make a tiny (negligible) modification of ω_0. (ii) We note now that $\omega_x(t)=-\gamma B_x(t)$ and $\omega_y(t)=-\gamma B_y(t)$ are periodic at the particle orbit frequency and its harmonics, so that the contents of the square brackets will be of the form $\omega_{xy}\sin[\phi\pm(\omega_0\pm\omega_r)t]$ and $\omega_{xy}\cos[\phi\pm(\omega_0\pm\omega_r)t]$. We note also that $|\omega_x|/|\omega_0|$ and $|\omega_y|/|\omega_0|$ are both $<10^{-3}$ for the situations of interest here. We conclude that the variation of dJ_z/dt is periodic and that after integrating $J_z(t)$ is also periodic with amplitude $<10^{-3}J_{xy}$, or $<10^{-3}J$, except on resonance where $\omega_r\to\omega_0$. Thus J_{xy} varies from the total J by less than 1 ppm and can be taken to be constant to a very good approximation. In view of the foregoing, we take J_{xy} to be constant and replace Eqs. (44) and (45) by

$$\frac{dS_z}{dt}=[\omega_x(t)\sin(\omega_0t)-\omega_y(t)\cos(\omega_0t)] \tag{46}$$

and

$$\frac{d\phi}{dt}=-S_z(t)[\omega_x(t)\cos(\omega_0t)+\omega_y(t)\sin(\omega_0t)], \tag{47}$$

where $S_z(t)=J_z(t)/J_{xy}$. The previously used Eqs. (35) and (36) are closely related to Eqs. (46) and (47).

The procedure for obtaining the cumulative phase change $\Delta\phi$ is now clear; first, $\omega_x(t)$ and $\omega_y(t)$ are found along the particle paths through $\mathbf{B}_{xy}(\mathbf{r})$ for parallel $\mathbf{E}$ and $\mathbf{B}_0$ fields. Then Eq. (46) is integrated and the result for $S_z(t)$ is inserted into Eq. (47) which is in turn integrated over the range $t=0$ to T. The Ramsey interval T spans a large number of orbital and Larmor periods. Finally, $\Delta\omega_{\uparrow\uparrow}=\Delta\phi(T)/T$.

The motion of the particle under consideration is projected onto the xy plane, where it moves in an orbit which is a polygon comprising a series of chord paths all of equal length. As in Fig. 3, the angle between the radius coinciding with the start of a chord and the radius passing through its center is called α.

We chose the x axis so that it passes through the center of the trap and has its direction of positive x passing through the center of the zeroth chord path that ends in the first collision with the sidewall. For the circulation sense $(+)$ the particle on this zeroth chord path will be traveling parallel to the y axis with y becoming more positive. The central reference point of the $n=1$ chord path, which follows the first collision is on a radius at an angle 2α to the x axis. Along the nth chord path we have

$$x_n(t)=R_c\cos A_n-R_sf(t)\sin A_n, \tag{48}$$

$$y_n(t)=R_c\sin A_n+R_sf(t)\cos A_n, \tag{49}$$

where $A_n=n2\alpha=\omega_r t_n$ and $\omega_r=\alpha v_{xy}/R_s$ from Eq. (27), and $R_s=R\sin\alpha$, and $R_c=R\cos\alpha$. The function of time $f(t)$ has a sawtooth form; at each collision, it flips instantaneously from 1 to -1, and then it rises linearly with time after the collision, just reaching 1 at the next collision. The first term on the right side of Eq. (48) represents the value of x at the midpoint of the nth chord path and the second term is the variable addition to x as the nth path is traversed. Soon, $f(t)$ will be replaced by its equivalent Fourier series. The velocity components of the nth path are

$$v_{xn}(t)=-|v_{xy}|\sin A_n,\quad v_{yn}(t)=|v_{xy}|\cos A_n. \tag{50}$$

Now $\mathbf{B}_{0r}=-(\partial B_{0z}/\partial z)\mathbf{r}/2$, so $B_x(x,y)=-(\partial B_{0z}/\partial z)x/2$ and $B_y(x,y)=-(\partial B_{0z}/\partial z)y/2$. In addition, there is $\mathbf{B}_v$ in the direction of $\mathbf{E}\times v$, whence $B_{vx}=-v_yE/c^2$, $B_{vy}=-v_xE/c^2$. It follows that on the nth chord path

$$\omega_{xn}(t)=P_c\cos A_n-P_sf(t)\sin A_n+Q\cos A_n, \tag{51}$$

$$\omega_{yn}(t)=P_c\sin A_n+P_sf(t)\cos A_n+Q\sin A_n, \tag{52}$$

where

$$P=\gamma R(\partial B_{0z}/\partial z)/2,\quad P_c=P\cos\alpha,\quad P_s=P\sin\alpha,$$

$$Q=\gamma|v_{xy}||E|/c^2. \tag{53}$$

We will now go through many steps to obtain an expression for the Larmor frequency shift $\Delta\omega_{\uparrow\uparrow}$ for orbit sense $(+)$. Later, the resulting expression will be adapted to other cases by modifying its arguments as follows: for fields $\mathbf{B}_0\mathbf{E}\uparrow\uparrow$ and orbit sense $(-)$ replace Q with $-Q$, for fields $\mathbf{B}_0\mathbf{E}\uparrow\downarrow$ and orbit sense $(+)$ replace Q with $-Q$, and in all cases for orbit sense $(-)$ replace α with $-\alpha$. One can check that these operations are sufficient for the purpose by examining the behavior implicit in Eqs. (39)–(55).

The function $f(t)$ can be written as a Fourier series;

$$f(t) = \sum_{k=1}^{\infty} 2b_k \sin C_k, \tag{54}$$

where

$$b_k = (-1)^{k+1}/(k\pi), \quad C_k = k\omega_1 t = \omega_k t, \quad \omega_1 = \pi|v_{xy}|/R_s. \tag{55}$$

The ω_k are taken to be positive for both senses of orbit. Substituting Eq. (54) into Eqs. (51) and (52) and applying trigonometric relations, leaving the sum over k to be implicit, leads to the results

$$\omega_{xn}(t) = P_c \cos A_n - P_s b_k \cos(A_n - C_k) + P_s b_k \cos(A_n + C_k) + Q \cos A_n, \tag{56}$$

$$\omega_{yn}(t) = P_c \sin A_n - P_s b_k \sin(A_n - C_k) + P_s b_k \sin(A_n + C_k) + Q \sin A_n. \tag{57}$$

There is a continuous dependence on t in the C_k. The angles A_n increase in discrete steps of size 2α at the times t_n of the collisions. Also,

$$t_n = (n^{-1/2})\Delta t = (n^{-1/2})(2R_s/|v_{xy}|). \tag{58}$$

We now insert Eqs. (56) and (57) into Eq. (46). Then by applying further trigonometric relations and assuming, just for the moment, that the A_n are constant over the time interval 0 to t of integration, we find, as needed for insertion into Eq. (47), that

$$\begin{aligned} -S_z(t) &= -S_z(0) + \left[\frac{P_c + Q}{\omega_0}\cos(D - A_n) - \frac{P_s b_k}{\omega_0 + k\omega_1}\cos(D + C_k - A_n) + \frac{P_s b_k}{\omega_0 - k\omega_1}\cos(D - C_k - A_n) \right]_0^t \\ &= -S_z(0) + [\Lambda_n(t)]_0^t, \end{aligned} \tag{59}$$

where $D = \omega_0 t$. To allow for a discrete change of A_n at each collision, the evaluation of the above integral must be made as a sum of separate integrals over segments 0 to t_1, t_1 to $t_2, \ldots, t_{n-1}$ to t_n, and t_n to t. Therefore we write

$$-S_z(t) = -S_z(0) + [\,\Lambda_0(t)|_0^{t_1} + \Lambda_1(t)|_{t_1}^{t_2} + \cdots + \Lambda_{n-1}(t)|_{t_{n-1}}^{t_n} + \Lambda_n(t)|_{t_n}^{t}]. \tag{60}$$

We will now add the negative of the lower limit for the t_n to t integral segment to the upper limit for the t_{n-1} to t_n segment and call the result $-\Delta S_{zn}$. The first term of the contributions to $-\Delta S_{zn}$ is

$$\begin{aligned} &(P_c/\omega_0)[\cos(D_n - A_{n-1}) - \cos(D_n - A_n)] \\ &\quad = -(P_c/\omega_0)2\sin(D_n - A_n + \alpha)\sin\alpha, \end{aligned}$$

where use has been made of the facts that D is a continuous variable and that $A_n = A_{n-1} + 2\alpha$. Treating the other contributions to $-\Delta S_{zn}$ from Eq. (59) similarly, we find that

$$\begin{aligned} -\Delta S_{zn}(t) = &-\frac{P_c + Q}{\omega_0} 2\sin\alpha\sin(D - A_n + \alpha) \\ &+ \frac{P_s b_k}{\omega_0 + k\omega_1} 2\sin\alpha\sin(D + C_k - A_n + \alpha) \\ &- \frac{P_s b_k}{\omega_0 - k\omega_1} 2\sin\alpha\sin(D - C_k - A_n + \alpha). \end{aligned} \tag{61}$$

The relations $C_{kn} = k\omega_1 t_n = k(n-1/2)\omega_1\Delta t = k(n-1/2)2\pi$ [see Eqs. (27) and (55)] show that the C_{kn} can be omitted provided the sine is multiplied by an extra factor of $(-1)_k$ which annihilates with the $(-1)_k$ already present in b_k. Hence, the terms of the second two lines of Eq. (61) can be combined to give $+[P_s\omega_1/(\pi\{\omega_0^2 - K^2\omega_1^2\})]2\sin\alpha\sin(D_n - A_n + \alpha)$. The implicit sum over k, from $k=1$ to ∞, can be carried out as follows:

$$\sum_{k=1}^{\infty} \frac{2\omega_1}{\pi(\omega_0^2 - k^2\omega_1^2)} = -\frac{1}{\omega_0}\left\{\frac{1}{\delta} - \frac{\cos\delta}{\sin\delta}\right\} = -\frac{1}{\omega_0}F_1(\delta), \tag{62}$$

where we have used the relations $(\pi\omega_0/\omega_1) = \pi\omega_0\Delta t/2\pi = \delta$ and Ref. [22], paragraph 1.217, using $x = i\omega_0/\omega_1 = i\delta/\pi$, for the summation. The final minus sign of Eq. (62) will cancel that to come from Eq. (63).

We note also that $D_n = (2n-1)\delta$, where $\delta = \omega_0\Delta t/2$ and Δt is the duration of a chord path and the zeroth half chord path has been allowed for. Hence $(D_n - A_n + \alpha) = \alpha - \delta + 2n(\delta - \alpha)$. We can sum over n for all the $-\Delta S_{zn}$ by using Eq. (63) of the series sum results:

$$\sum_{m=1}^{n} \sin(\beta + m\psi) = K_1 - \frac{\cos[\beta + (n + 1/2)\psi]}{2\sin(1/2\psi)}, \tag{63}$$

$$\sum_{m=1}^{n} \cos(\beta + m\psi) = K_2 + \frac{\sin[\beta + (n + 1/2)\psi]}{2\sin(1/2\psi)}, \tag{64}$$

where $K_1 = -[2\sin(\psi/2)]^{-1}\cos\{\beta + (\psi/2)\}$ and $K_2 = -[2\sin(\psi/2)]^{-1}\sin\{\beta + (\psi/2)\}$. For this application we identify ψ with $2(\delta - \alpha)$ and β with $(\alpha - \delta)$. The series sums (63) and (64) can be obtained by summing geometric series with complex terms of the form $\exp[i(\beta + m\psi)]$. Since n is the only quantity in Eqs. (63) and (64) that changes with time, we note that K_1 and K_2 are constants. They are of the order of unity, except very near the resonances. In this application K_1 and K_2 will be multiplied by other quantities such as (P_c/ω_0) which are of order B_{xy}/B_0 and less than 10^{-3}. The resulting constants are then of this order and can be absorbed into the arbitrary, but assumed to be similarly small, $-S_z(0)$. We can also absorb, in the same way, the leftover unpaired lowest limit of integration $\Lambda_0(0)$ finally converting $-S_z(0)$ to $-S_z^{\dagger}(0)$. The result of the sum is then

$$
\begin{aligned}
-S_z(t) = &+(\{P_c+Q\}/\omega_0)\cos(D-A_n)\\
&-(P_s b_k/\{\omega_0+k\omega_1\})\cos(D+C_k-A_n)\\
&+(P_s b_k/\{\omega_0-k\omega_1\})\cos(D-C_k-A_n)\\
&+(\{P_c+Q\}/\omega_0)G(\alpha)\cos(D_n-A_n+\delta)\\
&+(P_s/\omega_0)F_1(\delta)G(\alpha)\cos(D_n-A_n+\delta)-S_z^{\dagger}(0),
\end{aligned}
\tag{65}
$$

$$
\text{where}\quad G(\alpha)=\{\sin\alpha/\sin(\delta-\alpha)\}. \tag{66}
$$

The first three lines on the RHS of Eq. (65) have come from $\Lambda_n(t)$, while lines 4 and 5 have come from the summation up to t_n. With the exception of the constant $-S_z^{\dagger}(0)$ all the other five terms are oscillatory with time—the first three vary through $D\omega_0 t$ and n, while the next two vary through n only. The phases $(D_n-A_n+\delta)=(2n\delta-2n\alpha)$ progress in time in discrete steps but their average progress is like $(\omega_0-\omega_r)t$. The amplitude factor $G(\alpha)$ can become infinite at resonances where $(\delta-\alpha)=m\pi$ for any integer m. Of the six terms, excluding the constant, the first three terms may be thought of as the current terms and the last three as accumulation terms.

Having obtained $-S_z(t)$ in order to calculate the phase shift $\Delta\phi$ using Eq. (47) we see that we also need to use Eqs. (51), (52), and (54), to make in Eq. (47) the conversion

$$
\begin{aligned}
&[\omega_{xn}(t)\cos(\omega_0 t)+\omega_{yn}(t)\sin(\omega_0 t)]\\
&\quad=[P_c+Q]\cos(D-A_n)-P_s b_k\cos(D+C_k-A_n)\\
&\qquad+P_s b_k\cos(D-C_k-A_n)\equiv\Omega'(t,n,k).
\end{aligned}
\tag{67}
$$

We shall soon need the integral of $\Omega'(t,n,k)$ with respect to t which is

$$
\begin{aligned}
&[(P_c/\omega_0)+(Q/\omega_0)]\sin(D-A_n)-[P_s b_k/(\omega_0+k\omega_1)]\sin(D+C_k\\
&\quad-A_n)+[P_s b_k/(\omega_0-k\omega_1)]\sin(D-C_k-A_n)\equiv\Omega(t,n,k).
\end{aligned}
\tag{68}
$$

Now taking t_n and t_{n+1} as lower and upper limits of integration and summing over k, as in obtaining Eq. (65), we obtain

$$
\Omega(t,n)\Big|_{t_n}^{t_{n+1}}=\left[\frac{P_c}{\omega_0}+\frac{Q}{\omega_0}+\frac{P_s}{\omega_0}F_1(\delta)\right]2\sin\delta\cos(D_n-A_n+\delta), \tag{69}
$$

where we have used the relation

$$
\sin(D_{n+1}-A_n)-\sin(D_n-A_n)=2\sin\delta\cos(D_n-A_n+\delta).
$$

We now use Eq. (47) to calculate $\Delta\phi$ after n paths and the time lapse t_n and, hence, the average frequency contribution $\delta\omega_{\uparrow\uparrow}$ to ω_L over the interval 0 to t_n. These steps yield

$$
\begin{aligned}
\Delta\omega_{\uparrow\uparrow}=&\frac{1}{n\Delta t}\sum_{m=0}^{n-1}\left\{\left(-S_z^{\dagger}(0)+\left[\frac{P_c}{\omega_0}+\frac{Q}{\omega_0}+\frac{P_s}{\omega_0}F_1(\delta)\right]G(\alpha)\cos(D_m-A_m+\delta)\right)\Omega(t,m)\Big|_{t_m}^{t_{m+1}}\right\}\\
&+\frac{1}{n\Delta t}\sum_{m=0}^{n-1}\left\{\int_{t_m}^{t_{m+1}}\left[\frac{P_c}{\omega_0}\cos(D-A_m)-\frac{P_s b_k}{\omega_0+k\omega_1}\cos(D+C_k-A_m)+\frac{P_s b_k}{\omega_0-k\omega_1}\cos(D-C_k-A_m)+\frac{Q}{\omega_0}\cos(D-A_m)\right]\Omega'(t,m,k)dt\right\}.
\end{aligned}
\tag{70}
$$

The first line of Eq. (70) arises from the four accumulation terms of Eq. (65) for $-S_z(t)$. Within any one path, these terms are independent of t; thus, the integration over time during the path only requires the integral already carried out in Eq. (68) and the summation of the result over k given in Eq. (69). The second line arises from the four current terms in Eq. (65) that are dependent on t via D and the C_k.

The leading factor $1/n=1/t_n$ gets steadily smaller and n becomes a few thousand as t_n approaches the Ramsey time T. At the same time, the sum 1 to n of the integrals representing all paths up to t_n gives rise to some terms that oscillate about zero and do not grow with the number of paths, and to other terms that do grow steadily with the number of paths (i.e., as n, or $n+1/2$, or $n+1$, or $n-1$, etc.). These growing terms come to dominate the result and are the only ones of interest. In these terms the factor of n resulting from the summation cancels with that from $1/n\Delta t$.

We now look at all the terms in Eq. (70) on this basis. The integrations are all simple to do and involve cosine or sine functions or their squares and products. First power cosine and sine functions generate others after the integrations and yet others after the summation and give finally, no growing terms. Any in-phase elements of products of cosine and sine functions produce some constants after integration, which will produce growing terms on summation.

First, the constant $S_z^{\dagger}(0)$ after multiplying by the RHS of Eq. (69) gives three terms oscillating about zero that do not grow in the summation and are thus of no consequence. Second, we note that all the remaining cross terms in Eq. (70) that are to be integrated and then summed contain either P^2 or PQ or Q^2. These three types give contributions to $\delta\omega_{\uparrow\uparrow}$ that are proportional to E^0, E^1, and E^2, respectively, and they will be considered in that order.

The result of our calculation of the growing P^2 terms in Eq. (70) is that the frequency contribution $\delta\omega_{\uparrow\uparrow PP+}$ to ω_L caused by the $\mathbf{B}_{0xy}$ fields, when there is zero $\mathbf{E}$ field and orbit sense (+) is given by

$$
\begin{aligned}
\Delta\omega_{\uparrow\uparrow PP+}=&(P_c^2/2\omega_0)+(P_s^2/2\omega_0)F_2(\delta)+(1/2\omega_0)[P_c\\
&+P_s F_1(\delta)]^2 G(\alpha)[\sin\delta/\delta],
\end{aligned}
\tag{71}
$$

where

$$F_2(\delta) = 1/3 + \{(\delta/\tan\delta) - 1\}/\delta^2. \quad (72)$$

The sum over k leading to the form of F_2 involves

$$\sum_{k=1}^{\infty} \frac{p^4}{k^2(p^2-k^2)} = \sum_{k=1}^{\infty} \frac{p^2}{k^2} + \sum_{k=1}^{\infty} \frac{p^2}{(p^2-k^2)}, \quad (73)$$

p having been identified with ω_0/ω_1. The first term on the RHS of Eq. (73) sums to $\pi^2 p^2/6$, as in Ref. [22], paragraph 0.233, while the second term sum can be found from Eq. (62). The two contributions on the first line of Eq. (71) derive from the cross terms of line 2 in Eq. (70). Each involves $\cos^2(D-A_n)$, which is always positive and averages to $1/2$. The contributions of the second line, of Eq. (71) involving P_c^2, P_cP_s, and P_s^2, come from line 1 of Eq. (70). The result in Eq. (71) satisfies several tests. In the low-speed case, $|\omega_{rp}| = |v_{xy}|/R \ll |\omega_0|$ and $\omega_1 \ll |\omega_0|$ (UCN). The parameter $\delta = \omega_0 \Delta t/2$ is large. For a peripheral orbit, the dominant shift is $(P^2/2\omega_0)$ from the first term. It represents correctly the affect of the static field addition of $\mathbf{B}_{0xy}$ at the perimeter. For this case, the next most important term is that from P_c^2 in the second line it represents the GP effect caused by the apparent rotation of $\mathbf{B}_{0xy}$ seen by the particle as it orbits. This contribution when added to the first agrees with the RBS shift of Sec. II.

For an orbit which goes to and fro along the diameter, $\alpha = \omega_{rp}\Delta t/2 = \pi/2$, $P_c = 0$, and $P_s = P$. The dominant contribution to the shift is now the second term in Eq. (71) where $F_2 = 1/3$, except at the resonance spikes. Again this result represents correctly the average effect of adding a static field, which in this case increases linearly from zero at the center of the path up to its maximum at the periphery. The term on the second line involving P_s^2 has a leading term $(P_s^2/2\omega_0)$ $(\cot\delta/2\delta)$. This is small except at the resonance spikes, which have a dispersive shape.

We can also examine the high-velocity case where $|\omega_{rp}| = |v_{xy}|/R \gg |\omega_0|$ and $\omega_1 \gg |\omega_0|$. In a peripheral orbit the first term gives $(P_c^2/2\omega_0)$ as before. However, the first term of the second line with $(P_c^2/2\omega_0)$ has the angular factor $\sin\alpha \sin\delta/\{\delta \sin(\delta-\alpha\}$ which grows in magnitude and approaches -1 as δ becomes small, making a cancellation of the main terms. In this limit the shift of ω_L away from $\omega_0 = -\gamma B_{0z}$ in response to the $\mathbf{B}_{0xy}$ fields is seen to be strongly suppressed—a condition which applies to the Hg magnetometer used at the ILL.

As noted in Sec. II already, these P^2 terms are independent of Q and of the direction and strength of the **E** field and so do not give false EDM signals.

Cross terms, containing PQ, give contributions to $\Delta\omega_{\uparrow\uparrow PQ}$ that are proportional to E and change sign for $\Delta\omega_{\uparrow\downarrow PQ}$. These are false EDM signals. The first line of Eq. (70) gives the contribution of

$$\Delta\omega_{\uparrow\uparrow PQ1+} = 2Q/\omega_0^2[P_c + P_sF_1(\delta)]G(\alpha)\sin\delta/\Delta t, \quad (74)$$

which reflects the fact that $\cos^2(D_m - A_m + \delta)$ time averages to $1/2$. Next, we consider the second line of Eq. (70). Cross terms with PQ in the integrand contain the products $\cos^2(D-A_m)$, $\cos(D-A_m)\cos(D+C_k-A_m)$ and $\cos(D-A_m)\cos(D-C_k-A_m)$, respectively. From these only the terms containing $\cos^2(D-A_m)$ give growing terms with $\cos^2$ averaging $1/2$. Their overall contribution is

$$\Delta\omega_{\uparrow\uparrow PQ2+} = P_cQ/\omega_0. \quad (75)$$

Thus, for the $(+)$ orbit sense considered so far, by adding $\Delta\omega_{\uparrow\uparrow PQ1+}$ and $\Delta\omega_{\uparrow\uparrow PQ2+}$ and using of Eqs. (53), (58), and (72) we obtain the result

$$\Delta\omega_{\uparrow\uparrow PQ+} = \frac{PQ}{\omega_0}\left\{\left[\cos\alpha + \sin\alpha\left(\frac{1}{\delta} - \frac{\cos\delta}{\sin\delta}\right)\right]G(\alpha)\frac{\sin\delta}{\delta} + \frac{PQ}{\omega_0}\cos\alpha\right\}. \quad (76)$$

To prepare to calculate the d_{af} signals for an isotropic distribution of velocities we need to average over both orbit senses so we need $(\Delta\omega_{\uparrow\uparrow+} + \Delta\omega_{\uparrow\uparrow-})/2$. To obtain the equivalent of Eq. (76) for $\Delta\omega_{\uparrow\uparrow-}$—i.e., for the orbit sense $(-)$—we must replace Q by $-Q$ and α by $-\alpha$ in Eq. (76). Then, in going from Eq. (76) to this average, we find that the last term gives zero. The other terms both contain $G(\alpha)$. For the first term with $\cos\alpha$, $G(\alpha)$ [see Eq. (66)] is replaced by

$$[G(\alpha) - G(-\alpha)]/2 = \sin\alpha \sin\delta\cos\alpha/[\sin(\delta-\alpha)\sin(\delta+\alpha)],$$

while for the second term with $\sin\alpha$, $G(\alpha)$ is replaced by

$$[G(\alpha) + G(-\alpha)]/2 = \sin\alpha\cos\delta\sin\alpha/[\sin(\delta-\alpha)\sin(\delta+\alpha)].$$

Completing these transformations we find that

$$\Delta\omega_{\uparrow\uparrow PQ} = \frac{PQ}{\omega_0}\frac{\sin\delta}{\delta}\frac{[\sin\alpha\sin\delta\cos^2\alpha + \sin^3\alpha\cos\delta F_1(\delta)]}{\sin(\delta-\alpha)\sin(\delta+\alpha)} = \frac{2PQ}{\omega_0^2\Delta t}\frac{[\sin\alpha\sin^2\delta\cos^2\alpha + \sin^3\alpha\sin\delta\cos\delta F_1(\delta)]}{\sin(\delta-\alpha)\sin(\delta+\alpha)}$$
$$= \frac{PQ|v_{xy}|}{\omega_0^2 R\sin\alpha}\frac{\left[\sin\alpha\sin(\delta-\alpha)\sin(\delta+\alpha) + \frac{\sin^3\alpha\sin 2\delta}{2\delta}\right]}{\sin(\delta-\alpha)\sin(\delta+\alpha)} = \frac{PQ|v_{xy}|}{\omega_0^2 R}\left[1 + \frac{\sin^2\alpha\sin 2\delta}{2\delta\sin(\delta-\alpha)\sin(\delta+\alpha)}\right]. \quad (77)$$

The corresponding expression for d_{af} is

$$d_{af} = -\frac{J\hbar}{2}\frac{\partial B_{0z}/\partial z}{B_{0z}^2}\frac{v_{xy}^2}{c^2}\left[1+\frac{\sin^2\alpha\sin 2\delta}{2\delta\sin(\delta-\alpha)\sin(\delta+\alpha)}\right]. \tag{78}$$

In the adiabatic case (most UCN experiments) δ is quite large—typically 20 rad. This makes the last term in the square brackets small compared with unity except for narrow spikes with a dispersive shape at the resonances. Figure 7 shows very good agreement between the d_{af}, including resonances, from Eq. (78), and the numerical computations for the UCN case. The leading term of Eq. (78) is the same, including the sign, as that of Eq. (20).

In the nonadiabatic regime $|\omega_r|>|\omega_0|$, the speed of the particles has increased to the point where the angles $\delta=\omega_0\Delta t/2$ are small—typically 0.03 rad. In this limit, the last term of Eq. (78) has grown in magnitude and approaches the value $-(1+\delta^2\{2/3-1/\sin^2\alpha\})$. After the cancellation of the unit term there is a negative residue proportional to $-\delta^2$ which on substituting $\delta^2=\gamma^2{B_0}^2R^2\sin^2\alpha/v_{xy}^2$ becomes $-[(\gamma^2{B_0}^2R^2/v_{xy}^2)(3-2\sin^2\alpha)/3]$. This is the asymptotic form of the square brackets in Eq. (78) in the high-velocity nonadiabatic limit. Its α dependence can also be expressed as $(1+2\cos^2\alpha)/3$. Thus, all the results of Sec. IV C are embodied in Eq. (78) and we are sure now that the α dependence of d_{af} in this regime is the same for both closed and unclosed orbits.

The growing terms from Eq. (70) containing Q^2 represent the second-order $\mathbf{E}\times\mathbf{v}$ shifts. Line 2 of Eq. (70) has $(Q^2/\omega_0)\cos^2(D-A_n)$ where the time average of the $\cos^2$ factor is 1/2, leading to a Larmor frequency shift of $\Delta\omega_{\uparrow\uparrow QQ^2}=(Q^2/2\omega_0)$ independent of the **E**-field direction (true of all Q^2 terms) and orbit sense. It is equivalent to the addition of a static field B_v in the *xy* plane. Line 1 of Eq. (70) contributes the term

$$\Delta\omega_{\uparrow\uparrow QQ1+}=(Q^2/2\omega_0)G(a)[\sin\delta/2\delta]. \tag{79}$$

Deriving the average over the two orbit senses to obtain $\Delta\omega_{\uparrow\uparrow QQ^1}$ from Eq. (79) converts the $G(\alpha)$ to $[G(\alpha)+G(-\alpha)]/2$, as given above Eq. (77). Finally, we have

$$\Delta\omega_{\uparrow\uparrow QQ}=\Delta\omega_{\uparrow\downarrow QQ}=\Delta\omega_{QQ1}+\Delta\omega_{QQ2}=(Q^2/2\omega_0)[1+(\sin^2\alpha\sin 2\delta)/\{2\delta\sin(\delta-\alpha)\sin(\delta+\alpha)\}]. \tag{80}$$

The factor in square brackets of Eq. (80) also occurred in Eq. (78) for d_{af}. It has a $|v_{xy}|$ dependence in addition to the factor of v_{xy}^2 contained in Q^2. As before, the high-velocity limiting form for the contents of these square brackets is $-[(\gamma^2{B_0}^2R^2/v_{xy}^2)(3-2\sin^2\alpha)/3]$. If we average over α for an orbit occupancy appropriate to an isotropic distribution of velocities in the trap, the factor $(3-2\sin^2\alpha)/3$ yields 1/2. The low-speed and high-speed limiting forms of the shift are then, respectively, found to be

$$\Delta\omega_{\uparrow\uparrow QQ}=\Delta\omega_{\uparrow\downarrow QQ}(|\omega_r|\ll|\omega_0|)=\frac{\gamma^2v_{xy}^2E^2}{2\omega_0c^4}, \tag{81}$$

$$\Delta\omega_{\uparrow\uparrow QQ}=\Delta\omega_{\uparrow\downarrow QQ}(|\omega_r|\gg|\omega_0|)=-\frac{\gamma^2R^2\omega_0E^2}{4c^4}. \tag{82}$$

The transition between these two forms occurs in the region where $\delta=\gamma B_0R\sin\alpha/|v_{xy}|\approx 1$. The ensemble average $\sin\alpha$ is $8/(3\pi)$. In the UCN case, δ is of the order of 10, so UCN are are well represented by Eq. (81).

V. EFFECT OF INTERPARTICLE COLLISIONS

Analytical methods become rather harder to pursue when interparticle collisions occur, although we make some limited observations below. Our results in this section rest mainly on computer simulations. These were carried out for a cylindrical trap with $R=0.25$ m and an electrode separation $H=0.10$ m. In the case of diffuse reflections a standard Monte Carlo method was used to select the direction of the outgoing particles including the inevitable cosine factor. All of the simulations were carried out with a gradient $(\partial B_{0z}/\partial z)=1$ nT/m(10 μG/m) throughout the trap volume. This is about the smallest gradient that can be achieved reliably in the experiments in a μ-metal shielded region monitored with rather standard noncohabiting magnetometers such as those based on Cs. This gradient is also big enough to give sufficiently large signals from the simulations.

The simulations start individual particles all with the same initial direction of **J** corresponding to full polarization and integrate the classical equation (24) for the expectation of **J** as the particle moves through the local **E** and **B** fields. Most of the simulations were for motion confined to the *xy* plane since these go much more quickly. The reflections at the circular trap boundary could be set to be diffuse, or specular. An effective mean free path could be introduced by adding particle-particle collisions, each of which resulted in an isotropic distribution of outgoing velocities.

A. Nonadiabatic case $|\omega_r|>|\omega_0|$ and the effects of collisions

The first thing observed with the results of the simulations is that there was no dependence of the results on surface reflection law (completely specular or completely diffuse). We find this to be is a remarkable result. It is particularly useful, since all our analytic calculations, for this $|\omega_r|>|\omega_0|$ regime, are restricted to specular reflection. There was also agreement within the error between the computed results and the various equations we have produced for this regime in Secs. III and IV. The reflection of Hg atoms is likely to be diffuse, but again our experimental results for Hg given in Sec. VI show good agreement with Eqs. (37) and (78).

We have also used computer simulation for buffer gas collisions. A set of results is shown in Figs. 10(a) and 10(b) for the nonadiabatic case of ^{199}Hg. With a $\mathbf{B}_0$ field strength of 1 μT and a trap radius R of 0.25 m, as used at the ILL, the

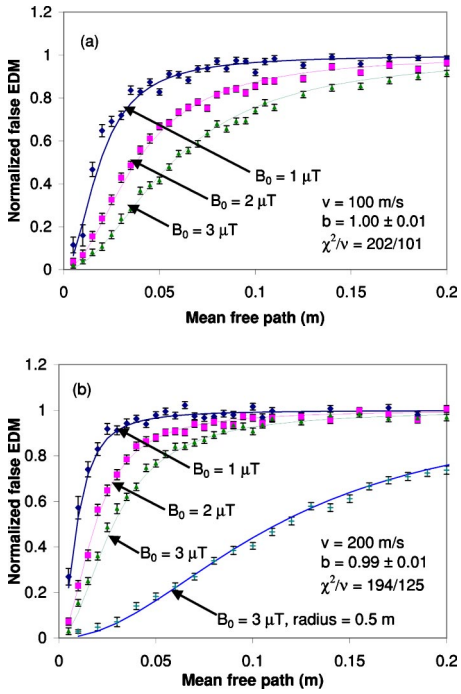

FIG. 10. (Color online) The suppression of the false EDM due to collisions with a buffer gas for the regime $|\omega_r| > |\omega_0|$. These simulated data, based on ^{199}Hg atoms in the neutron trap at ILL ($R=0.25$ m), indicate that on reducing the mean free path, the suppression amounts to a factor of 2 when the time taken to diffuse across the trap has increased to the point where it is similar to the Larmor period. (b) includes the case of a larger-radius trap. The data are normalized to the expected analytic value of false EDM when there is no buffer gas. The solid lines indicate an overall fit for all of the data within each figure to the function $[1+\{b \times 4R^2\omega_0/(2\pi v_{xy}\lambda)\}^2]^{-1}$ where b is a single free parameter.

simulations show that effective mean free path λ can be reduced to 0.025 m, or $R/10$, before there is any significant change in the size of the ^{199}Hg d_{af}. This is again a remarkable result, especially given that the radius of the trap determines the size of d_{af}. Simulations with 2 and 3 times stronger $\mathbf{B}_0$ fields show that the suppression of the d_{af} then takes effect at 2 and 3 times larger values of λ. These results suggest that the parameter for controlling the suppression is the ratio of the average time a particle takes to diffuse across the trap to the period of the Larmor precession.

For some insight into this criterion, we consider an idealized problem related to the case of traversing the trap diameter along the y axis with the spin along x discussed previously in Sec. IV C where the traverse was without collisions. Now we imagine that the particle executes a random walk with a collision-free path of about $R/10$ while remaining confined to the same diameter. It starts from one end and eventually it will reach the other end even if it returns to the start a few times. As it moves away from the start, J_z will start to increase from zero as for the free flight. However, any backward steps will be accompanied by some ramping down of J_z. There is a one-to-one correspondence between the rise of J_z and the progress of the particle across the diameter such that no matter how long random the walk takes before the eventual arrival at the far end, J_z will peak at the far end with the same value it would have had after a collision less free flight. At least, this is so when the duration of the walk remains much less than the Larmor period so that **J** does not precess too far from the x axis. We also note that the variation of B_y with position is the same regardless of whether the walk is random or not, and also that the longer the duration of the walk, the longer B_y can act on J_z to create J_y and to create the GP that J_y implies. Thus, the average the rate of creation of GP's not changed by the interparticle collisions occurring in a time short compared with the Larmor period. The condition just proposed concerning the Larmor period T_0 may be expressed as $(2R)^2/3D \approx T_0 = 2\pi/\omega_0$, where $D = v_{xy}\lambda/3$, is the diffusion coefficient. After rearrangement, the condition becomes $4R^2\omega_0/(2\pi v_{xy}\lambda) \approx 1$; it is fully consistent with the fitted function of Figs. 10(a) and 10(b), which show a suppression of the false EDM by a factor of 2 when the condition is met. The occurrence of the square of the parameter $[4R^2\omega_0/(2\pi v_{xy}\lambda)]$ in these fits ensures an asymptotic approach to maximal d_{af} when $\lambda \to \infty$ and to zero $d_{af\lambda}$ when $\lambda \to 0$.

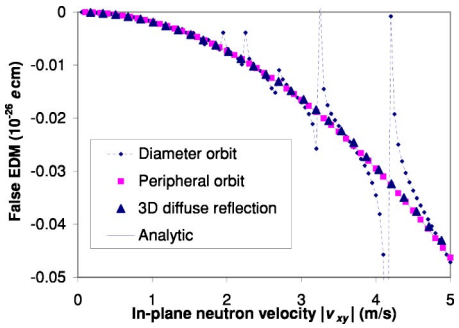

FIG. 11. (Color online) False EDM's obtained by computer simulation in the $|\omega_r| < |\omega_0|$ case. The results shown are for 2D specular reflection following peripheral and diameter orbits and for 3D diffuse reflection. The analytic result of Eq. (29) is shown as a smooth curve. Other parameters were $\partial B_{0z}/\partial z = 1$ nT/m and $B_0 = 1$ μT.

The nature of the fits also suggests that, in this non adiabatic regime, the asymptotic form of the expression for $d_{af\lambda}$ in the limit of high suppression will be

$$d_{af\lambda} \to d_{af}\left[\frac{\pi v_{xy}\lambda}{2R^2\omega_0}\right]^2 \quad \text{as } \lambda \to 0. \tag{83}$$

The actual case of the Hg magnetometer at ILL does depend on these results since up to 3×10^{-3} torr of ^{4}He gas is used to increase the strength of the **E** field used. At 3×10^{-3} torr, λ is estimated to be about 0.1 m for the ^{199}Hg to completely change direction. The conditions of Fig. 10(a) are the most apt with $B_0 = 1$ μT. The graph indicates a suppression of only 3% at a λ of 0.1 m.

B. Adiabatic case $|\omega_r| > |\omega_0|$ and buffer gas collisions

Again computations without buffer gas collisions show little dependence on the surface reflection law, except that the resonance spikes in d_{af} appear exclusively in the case of specular reflection. Away from these spikes the results are

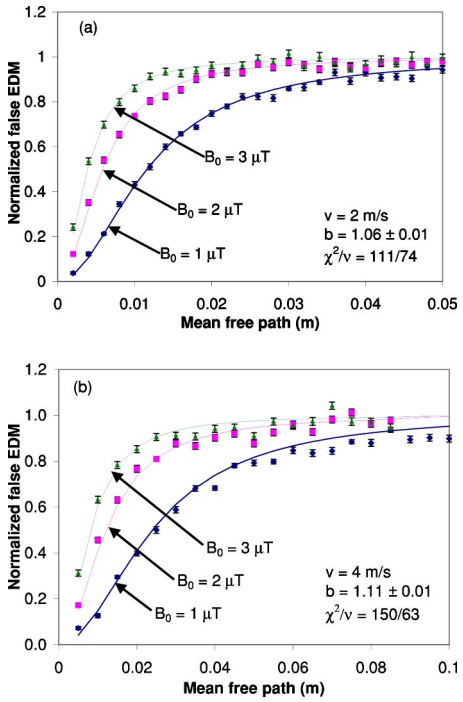

FIG. 12. (Color online) Suppression of the false EDM (relative to the expected value) caused by interparticle collisions in the regime appropriate to ultracold atoms and neutrons. The solid lines indicate an overall fit for all of the data within each figure to the function $[1+\{bv/(\omega_0\lambda)\}^2]^{-1}$ where b is a single free parameter.

independent of α and agree with Eq. (29). The whole simulation for perfect specular reflection is in very good agreement with Eq. (78) (see Fig. 9). The simulation for diffuse reflection shown in Fig. 11 is also in good agreement with Eq. (29).

The simulations with buffer gas collisions have adopted the conditions for trapped neutrons as used in the current *n*EDM measurements at ILL. Of course, a significant amount of buffer gas collisions cannot be used with UCN's without quickly knocking them out of the trap. However, the results we obtained may be relevant to trapped atoms or molecules. Some of the results are shown in Figs. 12(a) and 12(b). The suppression of the d_{af} becomes appreciable when the collision rate becomes higher than the Larmor frequency. This may be associated with too little settling time between the instantaneous changes of direction of the $\mathbf{B}_v$ that occur at each collision. The coherent build up of the GP then begins to be lost. The successful fit parametrization of Figs. 12(a) and 12(b) is consistent with this principle.

VI. CONNECTION WITH EXPERIMENTS

A. Measurements with ^{199}Hg and UCN at the ILL

False EDM signals have been observed in the Hg magnetometer used for the *n*EDM measurement at the ILL. They are observed indirectly as false *n*EDM's in the normal data processing which uses repeated measurements of $|(\omega_{Ln}/\omega_{\mathrm{LHg}})_{\uparrow\uparrow}|$ and $|(\omega_{Ln}/\omega_{\mathrm{LHg}})_{\uparrow\downarrow}|$. The $\omega_{\mathrm{LHg}\uparrow\uparrow}$ has $-2d_{af\mathrm{Hg}}E/\hbar$ added to it. Given that the magnetic moment of the ^{199}Hg ground state is positive, $|\omega_{\mathrm{LHg}\uparrow\uparrow}|$ is therefore, increased by $+2d_{af\mathrm{Hg}}E/\hbar$. When working with the ratios this is hard to distinguish from a decrease by $-(2d_{af\mathrm{Hg}}E/\hbar)|(\gamma_n/\gamma_{\mathrm{Hg}})|$ in $|\omega_{Ln\uparrow\uparrow}|$. The magnetic moment of the neutron is negative, so a d_{afn} would decrease $|\omega_{Ln\uparrow\uparrow}|$ by $-2d_{afn}E/\hbar$. If this really derives from $-(2d_{af\mathrm{Hg}}E/\hbar)\ |(\gamma_n/\gamma_{\mathrm{Hg}})|$, then

$$d_{af\mathrm{Hg}n}=\frac{|\gamma_n|}{|\gamma_{\mathrm{Hg}}|}d_{af\mathrm{Hg}}=\frac{\hbar}{8}|\gamma_n\gamma_{\mathrm{Hg}}|\frac{\partial B_{0z}}{\partial z}\frac{R^2}{c^2}\left[1-\frac{\omega_0^2}{\omega_r^{\dagger 2}}\right]^{-1}. \tag{84}$$

The data furnish a measure of $\partial B_{0z}/\partial z$ via a displacement Δh between the centers of mass (c.m.) of the UCN and the Hg caused by gravity, the c.m.$_{\mathrm{Hg}}$ being a few mm higher up than the c.m.$_{\mathrm{UCN}}$. This pulls the ratio $|(\omega_{Ln}/\omega_{\mathrm{LHg}})|$ away from the ratio $|(\gamma_n/\gamma_{\mathrm{Hg}})|$. In detail,

$$\left\{\frac{|\omega_n|}{|\omega_{\mathrm{Hg}}|}-\frac{|\gamma_n|}{|\gamma_{\mathrm{Hg}}|}\right\}\frac{|\gamma_{\mathrm{Hg}}|}{|\gamma_n|}=\pm|\Delta h|\frac{\partial B_{0z}/\partial z}{B_{0z}}, \tag{85}$$

where the + sign applies when $\mathbf{B}_0$ points downwards and the − sign applies when $\mathbf{B}_0$ points upwards. Introducing the ratio R_a given by $R_a=|(\omega_{Ln}/\omega_{\mathrm{LHg}})|/|(\gamma_n/\gamma_{\mathrm{Hg}})|$ into Eq. (85) gives

$$R_a-1=\pm|\Delta h|\frac{\partial B_{0z}/\partial z}{B_{0z}}. \tag{86}$$

Using Eq. (86) to substitute for $\partial B_{0z}/\partial z$ in Eq. (84) and omitting the square brackets of Eq. (84) as being close enough to unity, we find that

$$d_{af\mathrm{Hg}n}=\pm\frac{\hbar}{8}|\gamma_n\gamma_{\mathrm{Hg}}|\frac{R^2B_{0z}}{|\Delta h|c^2}(R_a-1). \tag{87}$$

The *n*EDM data provide two straight lines for d_{afn} plotted against (R_a-1) as shown in Figs. 13(a) and 13(b). The gradients, as given by a preliminary data processing, are $(1.85\pm0.37)\times10^{-26}\ e$ cm per ppm for $\mathbf{B}_0$ downwards and $-(1.78\pm0.35)\times10^{-26}\ e$ cm per ppm for $\mathbf{B}_0$ upwards. These signs are the same as those expected from Eqs. (85) and (87). The weighted average of the magnitudes of these slopes is $(1.81\pm0.26)\times10^{-26}\ e$ cm. We now increase this result by 2% to correct for the suppression from the average pressure of 4He buffer gas used and by another 2% to correct for the reduction caused by the direct GP false EDM of the UCN (see the next section). The corrected average slope for the $d_{af\mathrm{Hg}n}$ versus (R_a-1) is then $(1.88\pm0.26)\times10^{-26}\ e$ cm. Equating this with the modulus of the slope from Eq. (87) we find that $|\Delta h|=(2.73\pm0.39)$ mm.

Other measurements, using a similar trap, but with a variable electrode separation, so that known gradients $\partial B_{0z}/\partial z$ could be set up, provided a measure of the dependence of R_a on $\partial B_{0z}/\partial z$, and from that, the value $|\Delta h|=(2.81\pm0.11)$ mm for a UCN spectrum which is expected to be the same as that used in *n*EDM data taking. Thus, there is agreement between theory and experiment for the gradient of Fig. 13 that is well within the experimental errors. These values of $|\Delta h|$ also

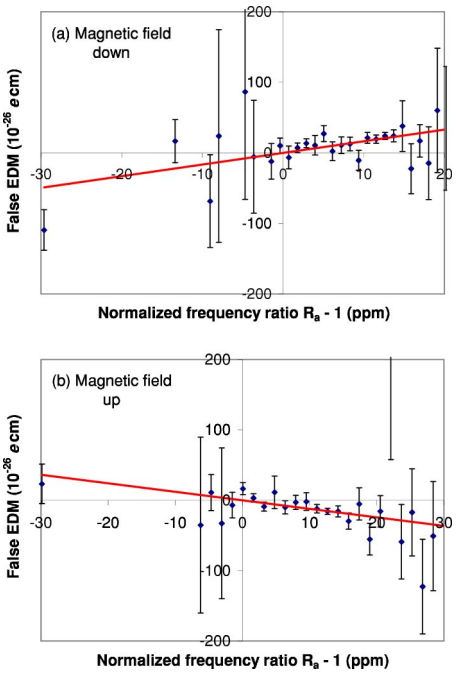

FIG. 13. (Color online) A subset of data from the neutron EDM experiment at the ILL, showing the measured false EDM as a function of the measured neutron to mercury frequency ratio. We expect this frequency ratio to be proportional to the magnetic field gradient. (Small, constant vertical offsets have been applied to the data in each plot.)

agree, to within 10%, with an estimate of $|\Delta h|$ from a phase space calculation of the UCN number density distribution over the 120 mm height of the trap.

B. Intrinsic false EDM's in experiments with UCN's

We now calculate the size of the intrinsic d_{afn} in the ILL measurements that arises out of the direct interactions of the fields with the UCN's. This d_{afn} exists independently of the use of the Hg magnetometer. Let us take the values $B_{0z}=1\ \mu$T and $\partial B_{0z}/\partial z=1$ nT/m. In the UCN case we need a value for $\langle v^2\rangle$. For ^{199}Hg the velocity is so high that the d_{af} is independent of velocity. We now remark that, for UCN's with a Maxwell spectrum $n(v)=3v^2/v_{\max}^2$, we find $\langle v^2\rangle=(3/5)v_{\max}^2$. After filling and emptying the trap, and storage in the trap for the Ramsey time T, about 2/3 of the original neutrons have been lost before detection and the velocity spectrum of those that remain has been softened. At that point $\langle v^2\rangle\approx(1/2)v_{\max}^2$ is a better representation. Finally we want $\langle v_{xy}^2\rangle=(2/3)\ \langle v^2\rangle=(1/3)\ v_{\max}^2$ for insertion into Eq. (29). The silica sidewall and 0.12 m height of the ILL trap make $v_{\max}=4.1$ m/s and $\langle v_{xy}^2\rangle=5.67$ (m/s)^2 (=$\{2.4$ m/s$\}^2$). With these values in Eq. (29), we find $d_{afn}=-1.1\times10^{-27}\ e$ cm. For the same field gradient, we find from Eq. (37) that $d_{af\mathrm{Hg}}=1.3\times10^{-26}\ e$ cm while from Eq. (84) that transferred from Hg to the neutrons is $d_{af\mathrm{Hgn}}=5.0\times10^{-26}\ e$ cm [and for a ^{3}He magnetometer, without buffer gas suppression, we would have $d_{af\mathrm{He}}=2.5\times10^{-25}\ e$ cm]. We note that, in the nEDM measurements at the ILL, the $d_{af\mathrm{Hgn}}$ transferred to the UCN from the Hg magnetometer is estimated to be −48 times that which the neutrons acquire intrinsically. Thus, the latter is only a −2% correction in our comparison between experiment and theory for $d_{af\mathrm{Hgn}}$.

If, in next-generation experiments, $v_{\max}$ was to be 7 m/s with $B_{0z}=1\ \mu$T, $\partial B_{0z}/\partial z=1$ nT/m, it is estimated that the d_{afn} would be $-3\times10^{-27}\ e$ cm, while such experiments aim to achieve nEDM errors of only $1\times10^{-28}\ e$ cm. It is clear that controlling this d_{afn} sufficiently puts significant constraints on the design. For example, increasing the strength of the $\mathbf{B}_0$ field, if homogeneity considerations will permit it, will help considerably. It is also evident that the best possible efforts will have to be made to control $\partial B_{0z}/\partial z$. Most of ILL nEDM data were taken with $|(R_a-1)|<1\times10^{-5}$. This translates into $|\partial B_{0z}/\partial z|<3$ nT/m. In fact it was possible, by virtue of the *cohabiting* magnetometer, to keep $|(R_a-1)|<1\times10^{-6}$, reducing the intrinsic $|d_{afn}|$ to $<3.3\times10^{-28}\ e$ cm. More sensitive magnetometers using ^{3}He atoms and/or UCN's and/or superconducting quantum interference devices (SQUID's) in the next-generation experiments are expected to make it possible to maintain even smaller gradients.

C. Other $\mathbf{B}_{0xy}$ fields with zero $\partial B_{0z}/\partial z$

We consider here, briefly, additional weak **B** fields that are everywhere parallel to the xy plane. If a weak uniform field lying in this direction is added to an existing $\mathbf{B}_0$, this simply tilts slightly the average direction of $\mathbf{B}_0$—i.e., slightly tilts the z axis and slightly changes the strength B_{0z}, the initial directions and values of which were, in any case, somewhat arbitrary. The overall $\mathbf{B}_0$ field would still be uniform and so the extra B_{xy} field would have no significant consequences for any of the foregoing calculations. Next, we consider a nonuniform steady field $\mathbf{B}_1$—for example, one with $B_{1z}=0$, $B_{1x}=qy$ and $B_{1y}=qx$ at all x,y,z. When $\mathbf{B}_1$ is added to a uniform $\mathbf{B}_0$, one sees by symmetry that the volume averaged $(\mathbf{B}_0+\mathbf{B}_1)$ is in the same direction as $\mathbf{B}_0$ and so the z axis is unchanged. However, there are some consequences from this addition. UCN's in the trap have an average precession rate which is close to that for the volume-averaged total field $|(\mathbf{B}_0+\mathbf{B}_1)|$ while to a very good approximation ^{199}Hg atoms in the trap have a precession rate which is determined by the z component of $(\mathbf{B}_0+\mathbf{B}_1)$ which is $\mathbf{B}_0$. As a result adding $\mathbf{B}_1$ to $\mathbf{B}_0$ moves the ratio R_a away and upwards from unity—a mechanism which does not depend on a finite $\partial B_{0z}/\partial z$. Thus, in using changes in R_a to estimate changes in $\partial B_{0z}/\partial z$ we have to assume either that fields like $\mathbf{B}_1$ are too weak to matter or that they are constant over the relevant period of time. It is a simple matter to calculate the shift in the ratio in the case of the $\mathbf{B}_1$ just specified. The first-order result is

$$R_a-1=\frac{q^2R^2}{4B_0^2}. \tag{88}$$

Thus, when $qR=1$ nT and $B_0=1\ \mu$T, R_a-1 is moved up from zero by (1/4) ppm, although $\partial B_{0z}/\partial z=0$. Our computer simulations shown in Fig. 14 have confirmed the validity of Eq. (88) to within the 2% accuracy of our assumptions about the responses of the UCN's and the ^{199}Hg to the B_{1xy} fields. When there is a finite $\partial B_z/\partial z$, the mechanism just discussed

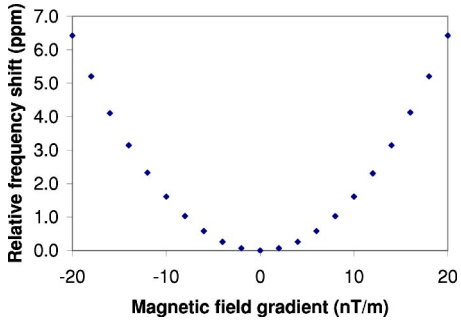

FIG. 14. (Color online) Results of computer simulations for the shift in the ratio $|(\omega_{Ln}/\omega_{\mathrm{LHg}})|$ with varying gradients q in a small $\mathbf{B}$ field, $B_z=0$, $B_x=qy$, $B_y=qx$, when it is added to a uniform $\mathbf{B}_0$ field of 1 μT aligned with the z axis. The shift is caused by the different averaging of B_x and B_y by the two species. These results are consistent with Eq. (88).

makes a finite contribution to the change in R_a in addition to that caused by any height difference between the two species. If we assume a uniform $\partial B_{0z}/\partial z$ and cylindrical symmetry, the shift is

$$R_a - 1 = \frac{p^2 R^2}{4B_0^2}, \tag{89}$$

where $B_r=pr$ and $p=(\partial B_{0z}/\partial z)/2R$. For $\partial B_{0z}/\partial z=1$ nT/m, $B_0=1$ μT and $R=1/4$ m, $(R_a-1)=(1/256)$ ppm. Given that this gradient would shift R_a by 3 ppm due to the species height difference, the effect given by Eq. (89) is negligible in comparison. (However, at 600 times larger gradients the two kinds of shifts would be similar in size.) Simulation results for a 20 nT/m gradient are shown in Fig. 15.

VII. CONCLUSIONS

We have developed some theories for estimating false electric dipole signals caused by geometric phases for trapped neutral particles with spins and magnetic moments. The particles are moving through static and nearly, but not completely, uniform $\mathbf{B}_0$ fields, seeing through their motion,

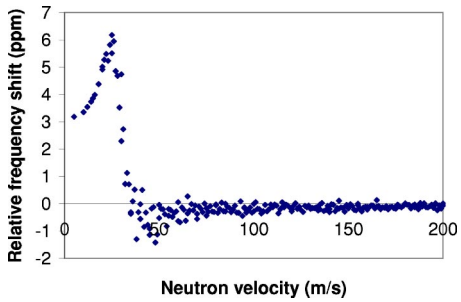

FIG. 15. (Color online) Results of computer simulations for the shift in the ratio $|(\omega_{Ln}/\omega_{\mathrm{LHg}})|$ with varying neutron velocity, when there is a gradient $\partial B_{0z}/\partial z=20$ nT/m in a $\mathbf{B}_0$ field of 1 μT. The shifts are caused by the different averaging, for the two species, of the B_x and B_y field components that must accompany this gradient. The shift at zero velocity is consistent with Eq. (89). When the neutrons travel as fast as the Hg atoms the shift becomes zero.

angular velocities of rotation of $\mathbf{B}_{0xy}$ components. The theory of Sec. IV B has established that when the particles are distributed uniformly over the volume of the trap with an isotropic distribution of velocities, the property of $\mathbf{B}_0$ that determines the size of the false EDM is the value of $\partial B_{0z}/\partial z$ when averaged over the volume of the trap, at least in the regime where the angular rotations of $\mathbf{B}_{0xy}$ are slower than the angular Larmor frequency. When the angular rotations of $\mathbf{B}_{0xy}$ are much faster, computer simulations suggest that this same property of $\mathbf{B}_0$ remains the relevant one, but we have no analytic proof in that regime. We have developed theories for the size of the false EDM in both regimes where $\partial B_{0z}/\partial z$ is uniform over the trap. Using simulations, it also been shown that, in both regimes, these false EDM signals can always be suppressed by having a sufficiently short mean free path caused by interparticle collisions. Nevertheless, we have found that in some conditions there can be very considerable shortening of the free path before this suppression begins. In the regime of high particle speeds, where they experience fast rotations of $\mathbf{B}_{0xy}$, we have observed the false EDM effect in real experiments that agree with the sign given in Eq. (37) and with the magnitude to within the error of 15% in the measurements. The theories presented predict that the false EDM effects can be large enough to put constraints on the design of current and future experiments to measure EDMs using traps.

ACKNOWLEDGMENTS

We would like to thank Larry Hunter and Norman Ramsey for stimulating us to examine this topic. We would also like to thank David Shiers for his many contributions to the building of the ILL *n*EDM experiment and also to thank members of the University of Washington EDM team for information on the construction of their ^{199}Hg systems. Support from the RFFI, via Grant No. 03-02-17305, is gratefully acknowledged by S.N.I. and Yu.S. Our program of neutron EDM measurements is supported by the UK Particle Physics and Astronomy Research Council.

APPENDIX A: MAGNETIC FIELD AREAS SWEPT ON TRAVERSING FREE PATHS

All the derivations here will average over both directions of travel. Thus the signs of the results will be absolute and appropriate to the chosen case of parallel $\mathbf{E}$ and $\mathbf{B}_0$ fields. The areas swept for the case of antiparallel fields can be obtained by reversing the sign of the areas obtained here. It should be understood that at all times when we talk about the path we are concerned with the projection of the path on the local xy plane. A path will have ends 1 and 2 at the sidewalls. First we will obtain the area $A_{sl\uparrow\uparrow}$ swept slowly and then the area $A_{i\uparrow\uparrow}$ swept instantaneously. We will adopt the notation $a_{\parallel}$ and $a_{\perp}$ for the components of $\mathbf{B}_{0xy}$ that are parallel and perpendicular to the path as projected onto the xy plane. One has also to include the motional field $\mathbf{B}_v$ given in Eq. (5), which always points in a direction perpendicular to the path and will be called $b_{\perp}$. The sense of these axes must be defined and maintained throughout the calculation. We adopt

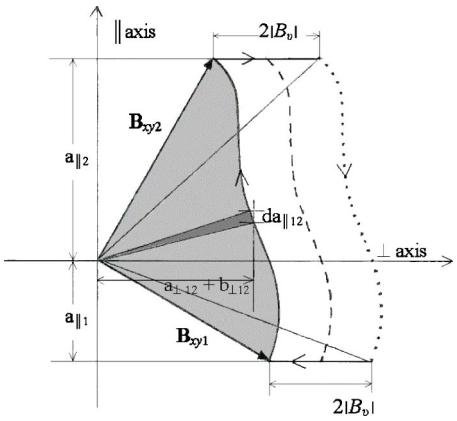

FIG. 16. (Color online) As a particle moves along the path from end 1 to end 2 the $\mathbf{B}_{xy}$ vector sweeps the shaded area. On returning from end 2 to end 1 the head of the $\mathbf{B}_{xy}$ vector passes along the dotted curve.

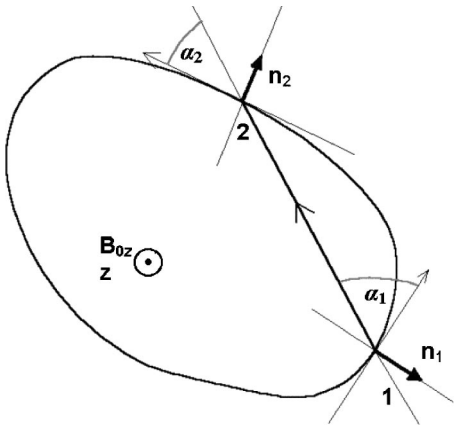

FIG. 17. (Color online) The angles α_1 and α_2, the tangents, and the normals at the ends of a path.

the vector $\mathbf{p}_{12}$ to represent the direction of the projected path in the sense $1\rightarrow 2$. A positive $a_{\parallel}$ will represent a field in the direction of $\mathbf{p}_{12}$, and positive $a_{\perp}$ and $b_{\perp}$ will represent fields pointing in the direction of $\mathbf{p}_{12}\times\mathbf{z}$. We choose to keep these same conventions when the path is followed in the sense $2\rightarrow 1$, so $\mathbf{p}_{21}$ will never be used. For the traverse $1\rightarrow 2$ we focus on a representative small element of the path. Traversing the small element sweeps the small area most darkly shaded in Fig. 16. To first order in small quantities and correct in sign this area may be written as $dA_{12}=(a_{\perp\,12}+b_{\perp\,12})\,da_{\parallel\,12}/2$. Because of our sign convention, traversing the same element of path in the sense $2\rightarrow 1$ gives $dA_{21}=(a_{\perp\,21}+b_{\perp\,21})\,da_{\parallel\,21}/2$. We now note that $a_{\perp\,12}=a_{\perp\,21}$, $b_{\perp\,12}=-b_{\perp\,21}$,and $da_{\parallel\,12}=-da_{\parallel\,21}$. The sign changes having come from the reversal of v_{xy}. It follows that

$$dA_{12}=(a_{\perp\,12}+b_{\perp\,12})da_{\parallel 12}/2, \tag{A1}$$

and

$$dA_{21}=(a_{\perp\,12}-b_{\perp\,12})(-da_{\parallel 12})/2. \tag{A2}$$

We now average over both directions of travel and obtain dA:

$$dA=(dA_{12}+dA_{21})/2=b_{\perp 12}da_{\parallel 12}/2=-|B_v|da_{\parallel 12}/2, \tag{A3}$$

where we have used $b_{\perp\,12}=-|B_v|$ which follows for parallel $\mathbf{E}$ and $\mathbf{B}_0$ fields and our axis conventions. Integrating for the whole path our final result $A_{sl\uparrow\uparrow}$ for the slow rotations is

$$A_{sl\uparrow\uparrow}=-|B_v|(a_{\parallel 1}+a_{\parallel 2})/2, \tag{A4}$$

where for this equation and its applications we have chosen to change our convention for $a_{\parallel}$ so that positive values of $a_{\parallel}$ at the ends always mean fields pointing *outwards* from the trap. We may regard the two contributions to the RHS of Eq. (A4) as being associated with ends 1 and 2, respectively.

It is convenient to resolve $\mathbf{B}_{0xy1}$ into normal and tangential components to the surface—namely, B_{0xyn1} and B_{0xyt1}. The latter, respectively, will be taken to be positive when in the direction of the outwards pointing normal $\mathbf{n}$ at end 1 and the the direction of the tangent $\mathbf{z}\times\mathbf{n}$. The equivalent components can be introduced at the end 2. Expressing Eq. (A4) in terms of these components, we obtain

$$A_{sl\uparrow\uparrow}=-(B_{0xyn1}\sin\alpha_1+B_{0xyn2}\sin\alpha_2)|B_v|/2-(B_{0xyt1}\cos\alpha_1-B_{0xyt2}\cos\alpha_2)|B_v|/2. \tag{A5}$$

The angles α_1 and α_2 are the angles (always taken to be positive) between $\mathbf{p}_{12}$ and the tangents to the surface $\mathbf{z}\times\mathbf{n}$ at the ends 1 and 2, respectively. They are shown in Fig. 17. For the cylindrically symmetric system that has been considered previously, the tangential components B_{0xyt} are zero and $\sin\alpha_1=\sin\alpha_2=\sin\alpha$, giving

$$A_{sl\uparrow\uparrow}=-B_{0R}|B_v|\sin\alpha. \tag{A6}$$

We now find the area swept in the instantaneous rotations of $\mathbf{B}_{xy}$ that are seen by a particle when it reflects from the sidewall at the ends of a free path. We assume that the reflection, on a microscopic scale at least, is specular. In this case the tangential component of v_{xy} is unchanged and the normal component is reversed. Thus only the normal component causes the instantaneous change of $\mathbf{B}_v$ and rotation of $\mathbf{B}_{xy}$. On leaving the surface at end one we assign only the change of the normal component from zero to v_{xyn1} $(=-|v_{xy}|\sin\alpha_1)$ as belonging to this path. The resulting change in $\mathbf{b}$—i.e., $\mathbf{B}_v$ in the tangential direction $\mathbf{z}\times\mathbf{n}$ at end 1 we will call b_{t1}. For parallel $\mathbf{E}$ and $\mathbf{B}_0$ fields $b_{t1}=-\sin\alpha_1|B_v|$. The components of $\mathbf{a}_1$ $(\mathbf{B}_{0xy1})$ and $\mathbf{b}_1$ in the direction of the outward normal $\mathbf{n}$ we will call a_{n1} and b_{n1}. The field area swept on departing from end 1 is $(a_{n1}+b_{n1})b_{t1}/2$ and for a particle going in the opposite direction the equivalent expression is $-(a_{n1}-b_{n1})(-b_{t1})/2$. The area, averaged over the two directions of travel, is $a_{n1}b_{t1}/2$. (The tangential components of $\mathbf{a}_1$ are in the same direction as the change of $\mathbf{b}$, and so do not affect the areas swept.) There is an equivalent result with the same sign at end 2, so after substituting for a_{n1} and b_{t1}, the total area swept instantly is found to be

$$A_{i\uparrow\uparrow}=-(B_{0xyn1}\sin\alpha_1+B_{0xyn2}\sin\alpha_2)|B_v|/2. \tag{A7}$$

In a cylindrically symmetric trap and field, this becomes

$$A_{i\uparrow\uparrow} = -B_{0R}|B_v|\sin\alpha, \tag{A8}$$

which is equal to $A_{sl\uparrow\uparrow}$ as given by Eq. (A6).

APPENDIX B: ORBIT WEIGHTING FACTOR FOR ISOTROPIC VELOCITIES AND UNIFORM NUMBER DENSITY

For an ensemble of particles having an isotropic velocity distribution and a uniform spatial distribution in the trap, the probability $P(\alpha)$ that a member of the ensemble will be in an orbit characterized by the angle α, as shown in Fig. 3, is

$$P(\alpha) = \frac{1}{\pi R^2}\int_{R\cos\alpha}^{R}\int_0^{2\pi} P(r,\alpha) r\, dr\, d\varphi = \frac{4}{\pi}\sin^2\alpha, \tag{B1}$$

where

$$P(r,\alpha) = \frac{2}{\pi}\frac{\dfrac{R}{r\sin\alpha}}{\sqrt{1-\left[\dfrac{R}{r\cos\alpha}\right]^2}}, \tag{B2}$$

and $P(r,\alpha)$ is the probability of α for particles found at radius r. Equation (B2) is derived from the trigonometric relation $r\sin\rho = R\cos\alpha$, as can be obtained from Fig. 18, with

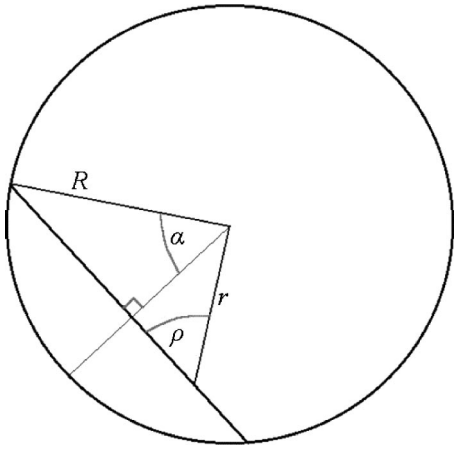

FIG. 18. (Color online) A chord path for a particle found at radius r. Also shown are the related angles ρ and α.

$$P(r,\alpha) = \frac{2}{\pi}\left|\frac{d\rho}{d\alpha}\right|, \tag{B3}$$

which relies on the fact that for an isotropic distribution of velocities the angle ρ is uniformly distributed.

[1] J. H. Smith, E. M. Purcell, and N. F. Ramsey, Phys. Rev. **108**, 120 (1957).
[2] E. A. Hinds and J. M. Pendlebury, Nucl. Instrum. Methods Phys. Res. A **440**, 471 (2000).
[3] C. J. Christenson, J. W. Cronin, V. L. Fitch, and R. Turlay, Phys. Rev. Lett. **13**, 138 (1964).
[4] K. Abe *et al.*, Phys. Rev. D **66**, 071102 (2002).
[5] B. Aubert *et al.*, Phys. Rev. Lett. **89**, 201802 (2002).
[6] S. M. Barr, Int. J. Mod. Phys. A **8**, 209 (1993).
[7] M. Trodden, Rev. Mod. Phys. **71**, 1463 (1999).
[8] B. C. Regan, E. D. Commins, C. J. Smidt, and D. DeMille, Phys. Rev. Lett. **88**, 071805 (2002).
[9] E. D. Commins, Am. J. Phys. **59**, 1077 (1991).
[10] N. F. Ramsey, *Molecular Beams* (OUP, London, 1956).
[11] M. Berry, Proc. R. Soc. London, Ser. A **392**, 45 (1984).
[12] N. F. Ramsey, Phys. Rev. **100**, 1191 (1955).
[13] F. Bloch and A. Siegert, Phys. Rev. **57**, 522 (1940).
[14] S. K. Lamoreaux, Phys. Rev. A **53**, R3705 (1996).
[15] P. G. Harris *et al.*, Phys. Rev. Lett. **82**, 904 (1999).
[16] I. S. Altarev *et al.*, Phys. At. Nucl. **59**, 1152 (1996).
[17] K. Green *et al.*, Nucl. Instrum. Methods Phys. Res. A **404**, 381 (1998).
[18] R. Golub and S. K. Lamoreaux, Phys. Rep. **237**, 1 (1994).
[19] Yu. Borisov *et al.*, Nucl. Instrum. Methods Phys. Res. A **440**, 483 (2000).
[20] E. Aleksandrov *et al.*, Proposal No. R-00-05.2 to P.S.I., 2003.
[21] J. Samuel and R Bhandari, Phys. Rev. Lett. **60**, 2339 (1988).
[22] I. S. Gradshteyn and I. M. Ryzhik, *Table of Integrals, Series and Products*, edited by A. Jeffrey (Academic Press, Boston, 1965).